Design of a Condenser-Boiler for a Binary Mercury-Organic Rankine Cycle Solar Dynamic Space Power System

Randy Michael Cotton, CPT
HQDA, MILPERCEN (DAPC-OPA-E)
200 Stovall Street
Alexandria, VA 22332

Final Report, 15 May 1987

A thesis submitted to the Massachussetts Institue of Technology, Cambridge, MA in partial fulfillment of the requirements for the degree of Master of Science, June 1987.

DESIGN OF A CONDENSER-BOILER FOR A BINARY MERCURY-ORGANIC RANKINE CYCLE SOLAR DYNAMIC SPACE POWER SYSTEM

by

Randy Michael Cotton

B.S., United States Military Academy

(1978)

SUBMITTED IN PARTIAL FULFILLMENT

OF THE REQUIREMENTS OF THE

DEGREE OF

MASTER OF SCIENCE

IN AERONAUTICS AND ASTRONAUTICS

at the

MASSACHUSETTS INSTITUTE OF TECHNOLOGY

June 1987

Signature of Author Randy M. Cotton

Department of Aeronautics and Astronautics

May 8, 1987

Certified by

May 7 1987

Professor Jean F. Louis

Thesis Supervisor

Accepted by Harold Wachman

Professor Harold Y. Wachman

Chairman, Departmental Committee on Graduate Students

DESIGN OF A CONDENSER-BOILER FOR

A BINARY MERCURY-ORGANIC RANKINE CYCLE

SOLAR DYNAMIC SPACE POWER SYSTEM

by

RANDY MICHAEL COTTON

Submitted to the Department of Aeronautics and Astronautics
on May 8, 1987 in partial fulfillment of the
requirements for the Degree of Master of Science in
Aeronautics and Astronautics

ABSTRACT

A theoretical design was performed for the condenser/boiler of a space-based solar dynamic power system. The base system is a binary Rankine cycle with mercury and toluene as the working fluids. System output is 75 KWe with a combined efficiency of 41.1%. Design goals were to develop the most reliable, mass efficient unit possible for delivery to a space station.

The design sized the unit based on toluene properties and used a computer generated heat balance to thermodynamically match the two fluids. Molybdenum was chosen as the material due to mass effectiveness in heat transfer, strength, and resistance to mercury corrosion. The unit transfers 137.46 kilowatts of thermal power and can operate at varying mass flow rates. Effectiveness in heat transfer is 0.96 and mass performance is 0.016 kg/KWth transferred. The design keyed on using only existing technologies and the results call for no new developments.

Thesis Supervisor: Dr. Jean F. Louis

Title: Professor of Aeronautics and Astronautics

ACKNOWLEDGEMENTS

Many thanks are extended to Professor Jean Louis for his patience and guidance while I stumbled, tripped, and eventually learned something. Also, thanks to all the open doors at M.I.T. The learning experience is tremendously enhanced when the asker does not have to claw through layers of buffers and secretaries.

TABLE OF CONTENTS

LIST OF SYMBOLS

Ae or A_E - effective area, Aw + Af·fe.

Af or A_F - fin area, f_L·L (one side, per unit length)

Aw or A_W - wall area, not counting extended surfaces

Cp - specific heat (J/kg-°K)

Dh - hydraulic diameter ($4 \cdot A_{FLOW}$/Perimeter)

dn, ρ - density (kg/m^3)

E - side effectiveness for heat transfer, f(Aw,Af,fe)

fe - fin effectiveness

f - friction factor

fl - fin length

fs - fin spacing

ft - fin thickness

h - heat transfer coefficient (W/m^2-°K)

i - enthalpy (Joules/kg)

k - thermal conductivity (W/m-°K)

L - length or length increment

m' - mass flow (kg/s)

m_U, μ - absolute viscosity (kg/m-s)

Nu - Nusselt number (Dh·h/k)

p or P - pressure (kPa unless otherwise indicated)

Pnet - shaft power (KW)

Pr - Prandtl number (m_U·Cp/k)

Q - heat transferred in an increment of heating length (W)

Re - Reynolds number (G·Dh/u)

sp - plate spacing

T - temperature (°K)

V - velocity (m/s)

v - mass specific volume (m^3/kg)

W - width of element

We - Weber number ($dn \cdot V^2 \cdot Dh$/suface tension)

x or X - vapor quality (percent of total mass flow in vapor)

SUBSCRIPTS

b or B - bulk quantity, based on free-stream average

w - wall, indicating the wall or at wall conditions

c - cold side value (toluene)

h - hot side value (mercury)

f - fin

t or T - total value, such as $A_T = A_F + A_W$

SS - steady state value

ST - start-up value

TP - two-phase flow parameter

FO - fluid or liquid only value, used in two-phase flow terminology

LV - difference between liquid and vapor value

L - liquid value

LIST OF FIGURES

LIST OF TABLES

CHAPTER 1 - INTRODUCTION

The next two decades are going to bring a new era to the space program in this and many other technologically developed countries, beginning with the construction of permanently manned orbiting facilities which will support research, commercial, and national interests. A significant development effort is underway to find less massive, smaller systems to provide the energy and power needs of the space station(s) than those utilized in the past.

Historically, many power generation systems have been used in space. The most popular, for unmanned mission scenarios, has been a combination of photovoltaics for power with batteries providing energy storage for peak/shadow periods. Fuels cells have also demonstrated good performance and monopropellant engines have been used for short duration missions.

The space station mission configuration calls for a low earth orbit (LEO), which will impose severe drag penalties for any system which must deploy a large amount of surface area, such as a photovoltaic array. Primarily for this reason, NASA is investigating the use of dynamic systems to support the power needs of the space station. Competitive cycles considered have been Brayton, Rankine, and Stirling cycles powered with either nuclear or solar thermal energy conversion.

Nuclear reactors have the disadvantage of requiring significant mass to shield personnel and sensitive components from radiation. The significant advantage to the solar dynamic systems is that their high efficiencies compared to photovoltaics mean that they require less extended surface area to intercept the amount of solar energy required to generate the same amount of power. This saves on fuel costs to overcome

drag, in mass costs required to support a smaller structure, and in overall launch costs.

The topic of this thesis is the thermal design of a condenser/boiler for a binary Rankine system. The general advantage of a Rankine system can be seen when compared to the Carnot cycle in Figure 1. Since the primary mechanism for thermal transfer is phase change, energy is added to or rejected from the system at a constant temperature. If the expansion in the turbine is of fairly high efficiency, the Rankine cycle can approach the maximum efficiency of the Carnot cycle. Additionally, since pumping a relatively incompressible liquid requires much less power than the compressor of a gas turbine (Brayton), the net available power from a given enthalpy change across the turbine is increased. The Brayton gas cycle also has the thermal disadvantage of transferring heat across a range of temperatures, which imposes a mass penalty on the radiator.

The idea of using a binary cycle to enhance overall efficiency has many possible advantages over a single cycle. The first is to extend the upper limit of organic Rankine cycles, which are limited by molecular breakdown at very high temperatures. Adding a topping cycle of another fluid can increase the peak cycle temperature (thus increasing system efficiency) while retaining the favorable characteristics of having an organic working fluid.

Probably the greatest potential benefit, and the best selling point, of a binary cycle is the possibility of cogeneration. Figure 2 illustrates the basic system configuration. Appropriate plumbing could potentially tap the fluid flows at any temperature level in the system. The possibility is to provide high quality thermal energy for environmental control, ovens, or experiments without going through the

inefficiency of thermal -> shaft -> electrical -> thermal power conversions. Fox [1] demonstrated that significant savings can be made in radiator and receiver masses if part of the total energy delivered is thermal provided at the radiator temperature.

While the exact power requirements of a manned space station can only be estimated at this point, it remains unlikely that a binary Rankine cycle will be used in the initial stage of station operation. However, as experience is gained in what the actual power requirements will be, a binary system may become very attractive as an expansion module when phasing the total power up from 75 to 300 KWe. The high attainable efficiencies (.38-.42) combined with cogeneration possibilities indicate the system could operate in the 30 - 50 Kg/KW range for power output.

The design concept of this thesis is to develop a condenser/boiler for the junction between the top and bottom cycles which has a flexible operating range of mass flow rates and enhances system reliability. The following analysis presents a mercury-toluene combined Rankine cycle operating to produce 75 KWe as an expansion module for space station deployment.

The following chapters of this thesis define the specific problem at hand by indroducing the fluid properties, reference cycle, and design configuration. Chapter 2 discusses the working fluids, performs a reliability analysis of various configurations, and presents the reference cycle. Chapter 3 demonstrates and selects appropriate heat transfer coefficients and performs initial sizing to determine the practical limits of the toluene side. Chapter 4 introduces the mercury two-phase flow model, performs a detailed heat balance, and thermally "matches" the two fluids. Final design configuration and performance are presented in

Chapter 5 along with detailed dimensions and fluid properties. Chapter 6 evaluates candidate materials and discusses possible assembly/ manufacturing techniques. Chapter 7 concludes with recommendations on the impact of altering the reference cycle and introduces a possible system configuration for employment. The Appendices contain detailed calculations for material which was summarized in the text and recommend an experiment to eliminate two areas of concern over heat transfer coefficients.

CHAPTER 2 - THE BINARY CYCLE

WORKING FLUIDS

The reference cycle for the binary system presented here is based on what are perceived to be the most reliable, well-tested, and proven technologies available. Fox [2] performed a study on the improvements of existing cycles and hardware to determine where proven technologies could be used to produce a more efficient, versatile system which is within the technology capabilities of this decade. For these reasons, toluene and mercury were selected as the working fluids for the combined systems.

Toluene (C_7H_8) has excellent thermodynamic properties in a Rankine cycle. Figure 3 shows the Temperature-Entropy plot of toluene with a Rankine cycle superimposed. It is readily noted that any vapor expansion occurs under "dry" conditions. Toluene has a relatively low critical pressure which implies favorable heating conditions. Some two-phase flow problems in zero gravity can be avoided by "boiling" the fluid at supercritical pressures. Among organic fluids, toluene has a high heat of vaporization (h_{fg} = 233.7 KJ/kg @ 1.75 MPa), which means that a large amount of energy can be transferred for over relatively small temperature range. Additionally toluene is a natural lubricant and current research initiatives indicate that it could be used as a common fluid for bearings and alternator cooling.

Mercury has extensive service as a dynamic working fluid, extending from topping cycles for steam turbines to the SNAP-8 space power development program. Figure 4 shows a Temperature-Entropy diagram representative of mercury. The superheat is provided to ensure a relatively dry expansion through most of the mercury turbine. While mercury has a few unfavorable properties - its heat of vaporization is low

compared with other liquid metals and its vapor pressure is high. The high vapor pressure is partially offset in the condenser, where its higher density gives better performance than alkali metals. Fox pointed out that, compared to water and the alkali metals, mercury has the highest energy transfer per unit of volume flow rate. Additionally, the low melting point is favorable in a system which may have to start up under extremely adverse temperature conditions.

While the properties of both fluids are to a large degree very favorable, a central issue is the fact that the technologies are developed. Mercury was tested for performance in vacuum and zero gravity in the SNAP-8 program. Sunstrand Aviation has developed what they consider a space-worthy organic Rankine cycle utilizing toluene [3]. The following analysis, in all cases, uses technologies which have been demonstrated.

REFERENCE CYCLE

The reference cycle is defined in the region of power output currently deemed likely for solar dynamic space power systems (below 100 KWe). The cycle will superimpose an already defined mercury cycle over a modified toluene cycle proposed by Sunstrand Aviation [3]. The procedure was to combine the two cycles with reasonable assumptions on pressure losses, turbine and pump efficiencies, and to match these with the appropriate mass flow rates to keep the system in thermal equilibrium.

The following are the salient features of Fox's cycle.

Mercury inlet temperature (turbine)	1033 °K
Toluene inlet temperature (turbine)	644 °K
Pinch temperature difference	10 °K
Mercury turbine efficiency	0.75
Bottom cycle temperature (radiator)	350 °K

Figure 5 shows a combined temperature-entropy diagram for the superimposed

cycles. The assumptions on the mercury cycle are; a 10% pressure drop through the boiler, 85% pump efficiency, negligible temperature and density changes through the pump, and zero pressure loss in the condenser. Later it will be shown that the condenser has a net pressure increase.

Vapor quality at turbine exit, which determines the net heat flux into the toluene cycle, is 0.852. The power and heat transfer rates were then determined. Values were calculated based on enthalpy changes as functions of temperature and pressure.

$P_{net}/\dot{m}'_{HG}$ = 78.51 KW/(kg/s) $Q_{out}/\dot{m}'_{HG}$ = 251.13 KWth/(kg/s)

The next step is to do much the same with the toluene cycle. Changes were made at the peak cycle point of the Sunstrand cycle. The lower conditions of temperature and pressure were maintained as rigid since Sunstrand has already developed a Rotary Fluid Management Device (RFMD) to operate in that range [4]. The peak cycle temperature is set at 644 ^{o}K, radiator at 350 ^{o}K, and pump and turbine efficiencies at 0.54 and 0.72, respectively. There are pressure losses of 10.7% in the regenerator, 10.4% in the "boiler", and 19% drop from turbine outlet to pump (including regenerator and RFMD). These figures represent the preliminary results from sizing the boiler for a higher pressure range.

As before, the figures of significance are again the heat flux from the mercury cycle and, the net shaft power, both per unit of mass flow.

$P_{net}/\dot{m}'_{TOL}$ = 144.99 KW/(kg/s) $Q_{in}/\dot{m}'_{TOL}$ = 554.00 KWth/(kg/s)

Matching the mercury cycle Qout with the toluene Qin and setting the total shaft output to 78.95 KW (75 KWe with alternator efficiency of 0.95) gives the mass flows of mercury and toluene as the solutions to two simultaneous equations.

Mercury mass flow = 0.54736 kg/s
Toluene mass flow = 0.24812 kg/s
Total output = 75 KWe
System efficiency = 0.411
Qin (Hg boiler) = 182.27 KWth
Qtransferred = 137.46 KWth

Table 1 summarizes the system state points as depicted in Figure 5. Under ideal conditions, the electrical output may be varied by varying the mass flows of the two fluids. The implied assumption is that the system components will perform equally well at the varying rates. Since the configuration will likely involve multiple turbines, as demonstrated in the reliability analysis, the boiler will be designed to perform at varying flow rates.

Table 1 - Reference Cycle State Point Summary

	Mercury		Toluene	
Point	Temp °K	Press MPa	Temp °K	Press MPa
1	654	0.156	350	0.034
2	655	5.56	354	5.17
3	963	5.0*	359.26	5.03
4	963	5.0	489.56	4.62
5	1033	5.0	644	4.14
6	654	0.156	538.5	.042
7			375	.038

*To simplify the analysis, the mercury boiler pressure loss was assumed to occur completely during the liquid phase.

RELIABILITY

A major concern over space deployment of binary solar dynamic system is reliability and system complexity compared with a single fluid system. Since a goal of this design is to enhance reliability, if possible, discussed below are possible heat exchanger configurations with a brief comparison of their impact on system reliability. At the end of this section the binary configuration is compared to a similar single fluid configuration to give an idea of the reliability "cost" of using the

binary cycle.

Figure 6 illustrates three possible configurations for the condenser/ boiler(s) in binary cycles. Each configuration uses four 25 KWe cycles for redundancy in producing 75 KWe. Even before an analysis is made, it can be seen that, in the event of a single turbine failure on the side of each fluid, configuration (c) is the only one which will allow any combination of failures while retaining 75 KWe output.

The following analysis uses an exponential failure distribution and assumes all failure rates to remain constant in time. While this cannot be strictly true, a valid comparison will still be drawn since the same conditions are assumed with all configurations. Figure 7 a-c detail the reliability networks of the three configurations in Figure 6. Set-up (a) has four independent systems in parallel with each other. Set-ups (b) and (c) are combinations of series and parallel, each having an additional unit which represents the valves required to direct the flow to/from the operating turbines from/to the operating heat exchangers. In the simplest possible form, these units can be modeled with one valve per heat exchanger, with the individual pumps controlling flow to/from the turbine assemblies (Figure 8). These elements affect the reliability of their configuration since they must be integrated in series. Providing redundancy/back-up for them means adding more valving, further reducing a series-type element's reliability, and will not be represented here.

The time scale used for the following calculations is five years. The time scale and the reliability below are arbitrary, since the time factor cancels out of the analysis when the configurations are compared. Current thinking and analysis are geared more towards a time scale of 7 to 10 years. However, the manned space station concept may very well change

traditional reliability thinking more towards shorter time scales which include recovery (repair) terms to account for the fact that on-site maintenance may now be possible. The manned capability may decrease the need for completely autonomous system operation throughout the life-cycle. The following definitions and relationships apply to an exponential distribution with constant failure rates [5]. Here "t" represents time, in years.

$$\lambda \text{ (failure rate)} = (1/R)(dR/dt) \qquad [1]$$

$$f \text{ (failure density)} = \lambda \cdot R = (1/m) \cdot e^{(-t/m)} \qquad [2]$$

$$R \text{ (reliability)} = e^{(-t/m)} = e^{(-\lambda t)} \qquad [3]$$

$$Q \text{ (unreliability)} = 1-R \qquad [4]$$

The reliability of n components with reliability, R

$$\text{Pr (all work)} = R^n$$

$$\text{Pr (one failure)} = n \cdot R^{(n-1)} \cdot Q$$

$$\text{Pr (less than k failures)} = \text{Pr (all)} + \text{Pr (one)} + \ldots + \text{Pr (k-1)} \qquad [5]$$

Each turbine, with components (alternator, RFMD, piping), is assigned a reliability of 0.9, which implies $\lambda = 0.021$/yr. Each valve is assumed to have R = 0.999, which implies $\lambda = 0.0002$/yr. $R(b)_{VLV} = 0.996$, $R(c)_{VLV} = 0.998$. Since the larger heat exchanger in configuration (c) will have a larger total cross section, a higher failure rate is assumed, since threat of micrometeoroid damage is proportional with exposed area. For comparison purposes, the failure rate of the smaller units (a and b) are 80% of the larger. For $R(c)_{EXCHANGER} = 0.95$ this implies $\lambda(c)_{Ex} = 0.01026$/yr and $\lambda(a,b)_{Ex} = 0.00821$/yr.

The reliabilities may now be evaluated by applying them to the networks in figure 7 and compared for impact on system reliability. It is

assumed that each configuration uses the same concentrator, receiver, and radiator. Failure is defined as system output less than 75 KWe.

Set-up (a) has a reliability of 0.784. Set-ups (b) and (c) have reliabilities of 0.883 and 0.892, respectively. Disregarding configuration (a) and comparing only the heat exchanger configurations of (b) and (c), without considering the turbines, R(b) = 0.9829 and R(c) = 0.9935. Translating this into failure rate, the set up in (b), with more reliable components, will fail 2.62 times as often as the system in configuration (c).

DESIGN CONCEPT

Based on the above analysis, the design approach for the condenser/ boiler will be to design a single unit to handle the entire load of a 75 KWe system. The unit will be designed to perform with varying flow rates to enhance off-design operation and to avoid difficulties with bringing turbines on/off line. Additionally, the design will allow stand-down of turbines during non-peak usage, scheduled maintenance, and replacement of defective components without shutting down the system. Specifically, the unit will be designed to operate at the design point over the range of mass flow rates corresponding to 50 to 75KWe power outputs and out of range performance will be predicted.

COMPARISON WITH SINGLE FLUID SYSTEM

Using the reliability from the above model (c), it is interesting to compare the above binary system with a single fluid system generating the same power output. Since there seems to be no justification to assume that the smaller turbines will have a more of less reliable than the larger (they are all quite small), turbine reliabilities are taken to be

0.90. Both the binary and the single fluid system could conceivably use the same heat collection and rejection system. Therefore, the reliability difference stems from the heat exchanger system and the fact that the binary system runs two sets of turbines instead of one. With these conditions, the single fluid failure density is approximately one-half that of the binary system, $f_{SINGLE}/f_{BINARY} = 0.501$.

Partially for the above reasons it is felt that the binary system is best suited as an expansion module for space station power. In future years, as the requirements for power become better defined, the cost savings of delivering a highly efficient, lighter weight, cogenerating power system will probably become very attractive compared to the increased risk associated with more turbines.

DESIGN COST FACTORS

Probably the most significant cost associated with the condenser/ boiler will be delivery costs to the space station. Using Johnson Space Center's Space Station Design Cost Factors [6], delivery of a non-pressurized unit (not including packaging) will cost $10,000 per cubic foot and $1000 per pound. If the condenser/boiler is assumed to be a very compact design of 10 kg, with an 80% void fraction (empty space), delivery to the space station will be $23,773 per unit, $22,046 of it being mass costs. This cost does not include protective packaging or installation tools/equipment.

Given the above cost factors, the design goal will be to minimize mass at every opportunity and minimize cube only where it is immaterial to total mass.

CHAPTER 3 - SIZING FOR TOLUENE

The material in this chapter introduces the heat transfer coefficient used for the supercritical heating of toluene, performs initial sizing of the heat exchanger based on toluene considerations, and selects the material for heat transfer surfaces. The approach is to design the exchanger one step at a time, eliminating assumptions and refining the accuracy of the design at each step. In this manner, it is hoped that the rationale for selecting the final design will be the result of a clear and coherent series of decisions.

HEAT TRANSFER COEFFICIENT

The choice of heat transfer coefficient for heating a supercritical fluid must be made based on the region of the temperature-entropy diagram the fluid is being heated in. Several tests have been conducted using water, carbon dioxide, and hydrogen. The correlation recommended by Swenson [7] is presented in equation 8 and is the correlation used by Sunstrand [8] in working with supercritical toluene.

$$Nu_W = h \cdot D/k_W = 0.00459 \cdot [(G \cdot D/\mu_{UW})^{0.923}] \cdot \cdot [(i_W - i_B)/(T_W - T_B) \cdot \mu_{UW}/k_W]^{0.631} \cdot (v_B/v_W)^{0.231} \quad [8]$$

The correlation is based on wall versus bulk properties where i is the mass specific enthalpy and v is the specific volume. Kays [9] points out that h is strongly affected by property variation and that it increases as the bulk temperature passes through the "transposed critical temperature", discussed below. Based on experiments with water and carbon dioxide, Griffith and Shiralkar [10,11,12] demonstrated that, under conditions of high heat flux (h > 500 Btu/hr-ft^2-^{o}F), supercritical Nusselt numbers are up to a factor of three below what would be expected using the McAdams

correlation (equation 6).

$$Nu = h \cdot D/k_B = 0.023 \cdot (Re_B^{0.8}) \cdot (Pr_B^{0.4}) \qquad [6]$$

Shiralkar drew his conclusions from the rates of change of velocity, temperature, and fluid density in the boundary layer. The main results are that the condition only exists with high heat flux and only when the bulk and wall fluid temperatures are not on the same side of the specific heat spike. The pseudo-critical or transposed critical temperature is that temperature corresponding to the maximum specific heat of a supercritical fluid at a given pressure. Griffith emphasizes that the condition disappears once the bulk temperature passes the spike. Shiralkar verified this and demonstrated that, when both wall and bulk temperatures are on the same side of the spike, the Nusselt numbers aligned very well with the McAdams correlation, even in the supercritical region.

The problem can be understood by referring to figures 9 and 10. Figure 9 shows the expected temperature and velocity profiles for turbulent flow from the wall to the centerline. If the pressure is assumed supercritical, and constant in cross-section, then figure 10 represents the average values of specific heat which might be expected as a function of temperature (distance from the wall). If the wall and bulk temperatures are on different sides of the specific heat spike, the sub-layer containing the very high specific heat will be in the boundary layer. The normal heat transfer relations using bulk conditions and $Q = m' \cdot Cp \cdot \Delta T$ will not accurately model the heat transfer.

The specific heat term in the Swenson correlation, as estimated by an enthalpy difference divided by a temperature difference, takes fair account of the problem. Whether the correlation is accurate for toluene

or not needs to be determined through experiment.

The conditions for the present problem are defined by the reference cycle. The wall temperature is consistently above the specific heat spike. The bulk fluid temperature is below the spike approximately three quarters of the temperature range and above it for one quarter. The average heat flux is expected to be high (on the order of 10000 W/m^2-^oK). If only one correlation is used, the average heat transfer coefficient will be too high. Since the toluene Re will increase with heating length, the exponential factor of 0.923 in the Swenson correlation will make this value too high past the specific heat spike. Since there is most likely some heat transfer degradation when the bulk temperature is below the spike, the McAdams correlation will be too high in that region.

Given the above considerations, the design heat transfer coefficient will be as follows. From inlet until the Cp spike is reached, the Swenson correlation will be used. From the spike to exit, the McAdams correlation will be used. This will present no difficulty with calculations since the toluene properties need to be recalculated at incremental lengths anyway.

SIZING THE EXCHANGER

Sizing a heat exchanger means finding a reasonable or desirable operating range in terms of dimensions which satisfy the heat transfer and allowed pressure drop for the fluids. Using an order of magnitude comparison, the three factors which influence heat transfer - the wall conductivity, mercury side heat transfer coefficient, and toluene side heat transfer coefficient - were compared. For thin walled passages the wall is (O) 10^5 W/m^2-^oK, the mercury is (O) 10^5 and the toluene is (O) 10^3-10^4. Since the toluene coefficient is smallest, its term will dominate the overall heat transfer coefficient

$$1/U = 1/h_{HG} + a/k_W + 1/h_{TOL}. \quad [7]$$

Equation 7 represents the general resistance model of heat transfer and "a" is the containment wall thickness.

Since the toluene thermal resistance dominates, the initial sizing is conducted based on toluene considerations alone, with reasonable assumptions on wall and fin conductivities and wall temperatures. Since toluene cannot be modeled as a perfect gas, and the properties vary dramatically along the heating length, a routine was prepared which interpolated the properties as functions of temperature and pressure. The tables of values used are detailed in Appendix A, and are integrated into the later programs as a subroutine. For the initial sizing, the properties were estimated with a linear temperature profile starting at 488°K and 4600 kPa and going directly to the assumed output values of 644°K and 4137 kPa. In this manner, all properties could be calculated as a function of temperature only.

The purpose of the first exercise was to find an acceptable operating regime for the fluid and establish trends for more detailed analysis. The toluene mass flow rate was set for the 75 KWe output and toluene side wall temperature was assumed at 650°K. Input variables were the initial fluid conditions and number and hydraulic diameter of tubes/passages. The program performed a detailed heat balance at each incremental length (5 cm), summed the incremental pressure loss and length, adjusted fluid temperature based on properties at section inlet and heat transfer from the wall, and recalculated properties for the next section before looping. Calculations ceased when the temperature reached 644°K, the pressure fell below 4100 kPa, or a prescribed maximum length was exceeded. Output variables were pressure loss, total length, inlet and exit Re.

The results of this "first cut" outlined certain trends and limits to the flow. In general, the smaller the Re, the smaller the pressure loss, the shorter the heating length, and the smaller the heat transfer coefficient. The best results were obtained at very small hydraulic diameters (Dh < 2mm), with large numbers of tubes, and low turbulent Re.

For the second iteration Rohsenow's "Basic Methods" [13,14] were modified for two averaged flow regimes in the boiler. Complete calculations are detailed in Appendix B. The first regime was for the fluid averaged properties from inlet to the specific heat spike and used the Swenson Nu correlation [Eqn 5]. The second was from the spike to outlet and used the McAdams correlation [Eqn 6]. The linear temperature-pressure profile was still assumed, transition for heat transfer coefficient estimated at 611°K, and wall temperature was assumed constant at 650°K. The input variables for this method are allowable pressure loss and hydraulic diameter. Output variables are total length per section, Reynolds number (if a restriction), and estimated number of tubes (based on a specified power output).

Since the first estimate indicated a favorable limit with low Re, the mass flow rate was prescribed for the 50 KWe power level. The reason for this is that, in later iterations, varying the power output will mean varying the G (mass velocity). The lowest Re (turbulent limit) will occur at the low power level. As the power is increased for a given system, mass flow rates, and hence G and Re, will increase. The limiting factor for the higher power level will be the overall pressure loss.

The results of this sizing indicate the direction the final design will need to proceed. In general, the more restrictive the allowed pressure loss, the shorter the heating length and the greater the number

of tubes/passages. The most favorable hydraulic diameters are in the range of 1 to 2.2 mm. This also implies a large number of flow passages. Heating lengths on the order of 5 meters are possible with insignificant pressure loss.

Preliminary conclusions lead to a methodology for final (accurate) sizing and practical limitations on the construction of the unit. Matching the allowed pressure loss in the two sections so that equivalent numbers of passages are used within a reasonable heating length indicate an approximate required heat transfer area of 2 m^2. For one of the reasonable heating length outputs, this would call for over 10,000 tubes to handle the 50 KWe flow rate. The required mass would be astronomical.

A preliminary estimate on the effect of employing extended surfaces was performed using Molybdenum as the passage material. With Dh = 1.5 mm, turbulent Re, and fin effectiveness of approximately 0.70, the estimate indicated that, for every percentage point of mass employed in extended surfaces (fins), almost a full percentage point of mass would be saved compared to an unfinned tube bundle with the same effective heat transfer area. This analysis was based on 70% of heat transfer area in fins. The implication is that optimum design will have a large percentage of heat transfer surface in toluene side finning. Likely configurations are finned plates or finned tubes with the toluene as the finned side fluid.

The final sizing step establishes correlations between the flow and heat transfer areas which would be "non-dimensional" in the sense that, if certain flow conditions could be met, the flow could be applied to various assembly geometries at will. Provided these geometries do not exceed the allowable pressure drop, and have the required effective area, they would be candidate designs.

The final sizing program, detailed in Appendix C, utilized an expanded program with input variables of hydraulic diameter (Dh) and mass velocity (G). Variables which did not affect the flow, but influenced heat transfer, were wall conductivity and fin effectiveness. Figure 11 illustrates the flow passage model. Square passages were assumed, fin length is equal to one half fin spacing, and fin thickness was varied so that fin effectiveness ranged above 0.50. A parallel flow was assumed and wall temperature was estimated based on the lowest turbulent Nusselt number for mercury measured by Rohsenow [15]. For a 1 mm wall thickness, Nu=8, and parallel flow, toluene side wall temperature will range from 649 to 652°K. 5Mo-Cr-V steel was used which has a thermal conductivity of 28.73 W/m-°K. With this geometry the effective heat transfer area per unit length is

$$Ae/L = 2\cdot(fs + 2\cdot fl\cdot fe) = 2\cdot Dh\cdot(1 + fe) \qquad [8]$$

for each flow passage, where fin effectiveness (fe) is a function of fin thickness, fin length, the material conductivity (k), and h_{TOL}. The unit was evaluated using a detailed heat balance for incremental lengths of 1 cm, with properties recalculated for every increment as a function of temperature and pressure. The heat transfer coefficient correlation was switched when bulk temperature passed 611°K, the estimated Cp spike. Output variables were total length, exit pressure, inlet and exit Re, and estimated number of passages for the 75 KWe power level. The reason for the higher mass rate is evident from the exit pressures - pressure drop is much less than expected. An additional routine performed an arithmetic average of the heat transfer and fin effectiveness as a function of the total length. Table 2 lists a few of the resulting values.

Table 2 - Toluene Sizing Output Values

Length (cm)	Exit Pressure (kPa)	G (kg/m^2-s)	Dh (mm)	h_{ave} (W/m^2-°K)	fe_{ave}	#tubes
92	4575	900	1.5	5107	0.7125	123
108	4575	900	1.7	5015	0.692	95
124	4574	900	1.9	4935	0.673	76
105	4526	1500	1.5	7868	0.626	74
123	4526	1500	1.7	7717	0.604	57
142	4524	1500	1.9	7604	0.583	46
115	4448	2100	1.5	10440	0.566	52
134	4448	2100	1.7	10250	0.543	41
155	4445	2100	1.9	10070	0.523	33

The flow trends are indicative of all values sampled. Several hundred samples were taken and general trends observed. Increasing G (with Dh constant) increases total length, decreases outlet pressure, and increases Re and h. Increasing Dh (with G constant) increases total length, marginally decreases output pressure, increases Re, and decreases h. A quantity which will be important later is the product of the tube length and the number of tubes. For a given geometry, this value scales the mass of the heat exchanger for different flow rates.

The utility of this form of data can be explained simply. The results of any one set of the above data can now be arbitrarily applied to various configurations to package it. Provided the total heating length, effective area, and hydraulic diameters are the same, the flow can be applied to various surface geometries to determine feasibility. The G and actual mass flow rate for the desired power level will scale the exchanger size by determining the number of passages required.

Before fitting the two flows together in a final geometry, it is necessary to eliminate one of the ambiguities by selecting a material for flow containment and heat transfer.

MATERIAL SELECTION

Historically, most specialized equipment has been manufactured with alloys because of the favorable properties offered by many of these materials. The choice of materials for a binary cycle heat exchanger is varied and the requirements are strenuous. The material must be resistant to mercury corrosion at elevated temperatures. Additionally, good thermal conductivity will enhance performance, and low mass will reduce delivery costs.

Recent advances in materials technology have made many materials available which have previously been nearly impossible to work with. Among these are pure metals which have very attractive strengths and transport properties, such as molybdenum and niobium.

A range of candidate materials is compared below. All of them have a history of use with thermal energy transfer and/or space applications. The method of comparison used was to evaluate their "mass effectiveness" for extended surface heat transfer. Using $q = A_E h(T_W - T_B)$, and assuming constant h and temperature difference (for a given cross section), then $q = (ct)A_E$. If it is further assumed that $A_F > A_W$, then $q \sim feA_F$. The following analysis evaluated several materials for fins which would produce the same heating length.

To compare them, a common flow passage was assumed. with constant fin spacing (1.5mm). Each was evaluated as a rectangular fin, with constant fin length (0.75mm), and the fluid flowing with a heat transfe· coefficient of h = 5000 W/m^2-^oK. The fin thickness for each was varied to obtain a fin efficiency of 0.70. The materials were then compared by cross sectional area and mass per unit length of fin. Table 3 summarizes the results.

Table 3 - Finned Heat Transfer Performance

Material	dn(kg/m^3)	Thick(mm)	k(W/m^2-^{o}K)	A_c(mm^2)	Mass/L(kg/m)
Copper	8954	0.045	363.4	0.068	0.0006
1%C Steel	7801	0.42	38.1	0.63	0.0049
Stainless	7817	0.82	19.9	1.23	0.0096
Molybdenum	10220	0.126	114.2	0.189	0.0019
Nickel	8906	0.265	60.6	0.398	0.0035

It should be noted that problems other than high mass can result from poor heat transfer performance. As fin thickness increases, losses from abrupt expansion and contraction will increase in magnitude as the flow is subjected to large accelerations and decelerations at inlet/exit.

Niobium was considered, but was not listed above due to its long-term creep performance, which is significant at high pressure over a wide temperature range [16]. While copper cannot be considered due to its incompatibility with mercury, its values are provided for comparison. Of the other candidates, Molybdenum wins by a large margin. It is very resistant to mercury, and has outstanding strength and thermal conductivity. In the temperature and pressure range of the condenser/ boiler all significant strength values are in the 100's of MPa [16,17].

For all remaining calculations and sizing efforts, Molybdenum will be used for wall, fin, and containment vessels. In addition to its mass advantage, its strength and high density make it a "compact" material, allowing a small volume for the heat transfer surfaces. Chapter 6 details the significant properties of Molybdenum and compares them with those of other candidate materials.

FINAL SIZING

Final sizing investigates the previously favorable hydraulic diameters and mass velocities when imposed on various passage geometries

of molybdenum finned passages. Table 4 lists some resulting values. The trends noted previously are still valid. Increasing G increases heating length but, at the same time, the required number of tubes is decreased. Increasing hydraulic diameter decreases the number of required tubes until about 1.5 mm, above which heating length increases.

Table 4 - Toluene Side Sizing with Moly Fins

Length (cm)	Exit Press (kPa)	G (kg/m^2-s)	Dh (mm)	fe_{AVG}	# tubes	Len·# (m)
118	4468	2000	1.547	0.658	25.1	29.6
108	4307	2000	1.412	0.659	27.9	30.1
101	4304	2000	1.320	0.657	30.1	30.4
94	4571	1000	1.547	0.769	50.1	47.1
86	4419	1000	1.412	0.768	55.7	47.9
80	4418	1000	1.312	0.767	60.2	48.1
78	4589	1000	1.254	0.733	59.1	46.0

The values in Table 4 represent about the limit that toluene can be pushed to using a "sizing" procedure. All values listed had a fin length of 2.75 mm and fin thicknesses of 0.68 mm. Hydraulic diameter was varied by varying the fin spacing. Increasing fin thickness from 0.68 has little effect on decreasing heating length, but can significantly increase the unit's mass. While the trends indicate that an optimum geometry will be obtained by maximizing the mass velocity and hydraulic diameter, the mercury flow will impose constraints. These constraints, combined with the values from the best performing toluene only sizing should provide an appropriate point from which to optimize the final design. The next chapter presents the mercury flow model and "matches" the thermodynamic and fluid flow properties of the two fluids.

CHAPTER 4 - MERCURY FIT

MERCURY FLOW MODEL

During the 1960's and early 1970's design and testing of liquid metal heat transfer and condensing components was performed for the SNAP space power programs. Of interest here are the test results of the various mercury condensing experiments and the performance of condensing equipment built in support of the SNAP-8 program [18,19]. Of particular interest are the results of tapered tube experiments where very high heat transfer coefficients were measured.

A summary of relevant test results follows. The Lockhart-Martinelli relations for two-phase flow were able to correlate a more than half of the pressure drop/momentum recovery data. For short condensing lengths (12-24 inches), the fog-flow, or homogeneous, model was almost a perfect fit [20,21]. Several of the studies showed that, for short condensing lengths, a fog completely filled the chamber with no observable film, down to vapor qualities less than 4% [22,23].

Many of the experiments were based on "wetting" or "non-wetting" condensation. It is interesting to note some of the problems the experimenters had in controlling film growth. In one of the wetting (film condensation) experiments [22], the experimenters had a difficult time promoting wetting and, when they did, the film remained uniformly thin and would not grow as predicted. In another experiment [19] experimenters could not get rid of the film, yet their data correlated with a non-wetting flow. In both of the above cases the vapor velocity seems to have controlled film growth and droplet entrainment. Generally, tapered tubes kept the velocities high and film growth to a minimum for longer lengths than constant diameter tubes.

Heat transfer performance predictions were not nearly as accurate as pressure drop (or rise) correlations. Predicted values of condensing film coefficient varied from 1200 - 22,000 Btu/ft^2-^{o}F. Measured results ranged from 22,000 - 117,000 Btu/ft^2-^{o}F, in one case as high as 147,000 Btu/ft^2-^{o}F (tapered tubes). While condensing heat transfer correlations are still unreliable and not generally accurate, a look at the model used is enlightening. For the most part, the heat transfer model assumed a growing film, transitioning from laminar to turbulent along the condensing length. The driving force was assumed to be the temperature gradients at the liquid-vapor interface and in the liquid film. Constant pressure, and therefore constant saturation conditions, were assumed. This author could find no reference where the saturation conditions were adjusted to account for variations in local pressure, although one experiment [19] plotted the estimated effect on saturation temperature.

Tabulated test results showed a remarkable variation with local static pressure. This is understandable since, at the microscopic level, it is actually the pressure gradient which allows a particle/molecule of vapor to overcome the surface tension of a droplet. Without attempting an analysis with pressure tensors, it it simply pointed out that the test data demonstrated highest condensing transfer coefficients when a positive pressure gradient existed along the flow length. Additionally, highest rates of condensing heat transfer coefficient (117,000) occurred for short condensing lengths with no observable film growth.

Based on the above discussion, the mercury flow model for the present design is a homogeneous two-phase flow model. All calculations will treat the two-phase flow as a single phase mixture with corrections based on quality to average the fluid properties. Appendix D gives the complete

mathematical formulation and equations used. The significant points are; vapor and liquid velocities are assumed equal, friction losses are calculated for liquid flowing alone and adjusted by a two-phase correction factor, and momentum pressure recovery is calculated from the bulk change in mass velocity as a function of geometry and quality changes along the condensing length.

The condensing coefficient will be

$$h(z) = h_{FO} \cdot (v_M/v_L)^{1/2}, \qquad [8]$$

which is a two-phase coefficient based on adjusting the liquid only rate ($_{FO}$) by the square root of the ratio of mean specific volume to the liquid only volume [24]. While this correlation is normally used for steam, it matches the results from the mercury tests very well. The liquid metal correlation of Cohen will be used for the liquid only value [25].

To try to duplicate the conditions from the best results measured during the SNAP performance tests and provide a reasonable amount of conservatism to the calculations, the following conditions are imposed. Minimize condensing length - this "rapid" condensation will decrease the likelyhood of unstable flow conditions. Provide a positive pressure gradient along condensing length - this will enhance condensation at all liquid-vapor interfaces. If/when calculated value of h(z) is greater than 600,000 restrict it to 600,000 $W/m^2\text{-}^oK$ - this will provide a conservative value of the condensing coefficient.

MATCHING THE TWO FLUIDS

There are several constraints to be imposed on any configuration involving the two fluids. The first of these have already been demonstrated by sizing the exchanger based on toluene alone. Minimum heating lengths and pressure drop involve mass velocities on the order of

2000 - 2200 kg/m^2-s and hydraulic diameters around 1.4 mm. Other constraints, involving the mercury flow are; maintaining turbulent flow conditions, prescribing outlet hydraulic diameter to be less than a critical value, keeping the mass velocity below a critical rate, and maintaining high but subsonic vapor velocities to enhance momentum transfer and liquid entrainment.

Of the above constraints, only two fall out without considering geometry - maximum velocity and critical mass velocity. Using inlet vapor conditions as worst case (highest velocity), the speed of sound, a = 255 m/s [$(dp/do)_s$]. The critical mass rate, based on L/D > 12, is calculated from Griffith's two-phase correlation [26] using the reference cycle outlet pressure, G = 25,100 kg/m^2-s.

The critical diameter used for the SNAP design was based on a Bond number which contains a gravity term. Another correlation, which uses the ratio of droplet critical height of condensation to the local tube diameter, is a function of vapor Weber number and is used here [27].

$$D_{DROP}/D_{TUBE} = 1/We < 1/2 \qquad [10]$$

This form can be rearranged and presented as a function of mass velocity and passage diameter to provide a maximum diameter at the interface (0% quality) or exit. Maintaining turbulent flow conditions is primarily a function of geometry, since the mass flow rate is defined by the reference cycle requirements.

Equation 11 is the base equation for matching the heat transfer between the two fluids. This form is selected because it has all the important variables together in the third term. If a cold side overall heat transfer relation were used, variable terms would appear in both the second and third terms. The overall (hot side) heat transfer coefficient

is

$$1/U_H = 1/(E_H \cdot h_H) + a/[(A_W/A_C) \cdot k_W] + 1/[(A_C/A_H) \cdot E_C \cdot h_C] \quad [11]$$

The side effectiveness for heat transfer is a function of geometry and extended surface effectiveness.

$$E = 1 - (A_F/A_T) \cdot (1 - fe) \quad [12]$$

Equation 12 is the same form as Kays and London's η_o [28] and has the same meaning as Rohsenow's effectiveness [29]. The heat transfer rate is given by the reference cycle (137.46 KWth) and the log-mean temperature difference is 55.3 °K. It should be noted that the logarithmic-mean temperature difference is not a valid evaluation parameter when applied to the toluene flow. It is used in the following discussion only to compare possible geometries. The cold side heat transfer coefficient can be estimated from the toluene sizing effort, E_H and (A_H/A_W) are unity (no mercury side finning), and overall heat transfer can be estimated by

$$q = A_H \cdot \Delta T_{LM} \cdot U_H \quad [13]$$

as a function of the above values and hot side area. Equations 11-13 provide the means of evaluating the required hot side area as a function of known values for a given geometry. Once the hot side area is known, the complete geometry can be defined in terms of A_C/A_W and the flow parameters.

Table 5 - Heat Transfer Influence Parameters

	Parameters			
increase	Dh	h_C	A_C/A_H	E_C
Fin Thickness			-	+
Fin Length	+	+	+	-
Fin Spacing	+	+	-	-
Mass Velocity		+		-

Without assuming a particular geometry, but using a thin, highly conductive wall, it can be seen that the driving factors are the three in

the last term of equation 11. The three are not independent of one another. Table 5 demonstrates the impact that varying one flow or geometry parameter will have on the other parameters.

If the rightmost term in equation 11 can be made on the order of 1/60000 (h_C=10000, A_C/A_H=10, E_C=0.6) with mercury and the wall on the order of 1/200,000, then the hot side area will be on the order of 0.07 m^2. This limiting case is probably unattainable because of the inter-relationships demonstrated in Table 5. The objective of fitting the two fluids together is to optimize the heat transfer area to transfer 137 KWth from mercury to toluene in the lowest mass/smallest volume configuration possible. The toluene sizing effort has already given an indication of minimum heating length and flow parameters. The next step is to compare various geometries for compatibility and to evaluate their pressure drop and heat transfer performance to select the most mass and volume efficient arrangement.

The first configuration considered is shown in figure 12. This is a tube and shell arrangement, either parallel or counterflow. Since the extended surfaces are needed on the toluene side, toluene is the shell fluid with mercury condensing inside the tubes. For determining feasibility, the tubes are assumed to remain at constant diameter.

The counterflow arrangement fails to meet the needs of the condenser-boiler on several counts. To minimize the hydraulic diameter of the toluene side, the effect of the extended surfaces is decreased as individual fin length is decreased in proportion with tube spacing. Referring to equation 11, this has the effect of decreasing the cold to hot side area ratio, minimizing the effects of the extended surfaces.

If additional finning is added to decrease the toluene side hydraulic

diameter, a limit is reached where the outside of the tube is completely covered with fins. Besides potential construction problems, this heavily finned tube requires a larger outer diameter as more fins are added. Larger diameter tubes imply fewer tubes to keep the mass velocity high enough for turbulent flow. In the region where the diameter of the tubes is large enough to enhance cold side effectiveness and keep toluene Dh low, the total toluene flow area is too large to maintain turbulent flow and heating length will increase. In the region where flow rates are high enough, the dimensions of the tubes and fins becomes ridiculously small. Besides assembly problems, the high number of tubes/passages cause the exchanger's mass to increase dramatically. In summary, tube and shell counterflow is deemed inappropriate, finned or unfinned.

The second concept evaluated was a finned tube cross flow arrangement such as that depicted in figure 13. Again, mercury is condensing inside the tubes and toluene is flowing through the finned passages. Starting with reasonable mercury diameters of around 5 mm, the number of passages to keep turbulent exit conditions is 15. The toluene hydraulic diameter is approximately twice the fin spacing. The cold to hot area ratio is a function of the number of fins per length of tube and tube spacing. In an equilateral triangle arrangement such as figure 14, the fins can be approximated as circular with length (r_o-r_i) as half the distance to the adjacent tubes.

This geometry potentially provides the best A_C/A_H ratio. From a simple heat balance point of view, the required hot side area is 0.14 m^2, which approaches the previously mentioned minimum. The drawback of this configuration is the number of toluene passes required (over 100). The toluene pressure drop due to turns alone will be more than 20% of inlet

pressure. Toluene heating length is also higher than desired, being more than 10 meters with all the passes. Therefore the finned tube cross flow is also deemed unfeasible since any action taken to correct the pressure drop will increase the unit's cube and, ultimately, mass.

The elimination of the above configurations leads to the plate-fin type geometry used to size the toluene. The original reason for selecting the plate-fin model was due to the earlier favorable results at low hydraulic diameters. These small diameters imply a large number of tubes or passages. A large number of tubes is massive and assembly difficulties will increase with shrinking tube size. A plate-fin arrangement, illustrated in figure 15, allows optimization of the parameters in equation 11 and total heat transfer area and mass may be minimized. If the pressure drop is reasonable, as expected, two or more toluene passes may be possible. Multi-pass will reduce the largest dimension of the exchanger, which is length. This will be important when a protective shell is put around the unit, since the mass of the shell will scale directly with the exposed surface area.

DETAILED HEAT BALANCE

The model used to evaluate the plate-fin configuration is a detailed heat balance between the mercury and toluene flow. As already discussed, molybdenum was selected as the wall and fin material due to mass effectiveness per unit length of fin. The program, detailed in Appendix E, performed a numerical integration along incremental lengths of flow passage. At each incremental length a detailed heat balance was performed using the hot side reference of equation 11 to calculate total heat transferred, Q. This was balanced against the bulk inlet temperature of toluene and inlet fluid properties to calculate a new temperature for the

next section,

$$T_{NEW} = T_{IN} + Q/(\dot{m}' \cdot Cp). \qquad [14]$$

It should be pointed out that the T_{NEW} calculated is a pessimistic value. Since the interpolation routine calculates the specific heat by averaging two to four known values, and the actual Cp is on a smooth curve with a steep slope, the calculated value is higher than the true value. This results in slightly less temperature change in equation 14 than would actually be achieved. Based on heat transfer a new quality value for the mercury flow was calculated. Using the friction factor, $f = 0.046/Re^{0.2}$, and

$$dP = 4 \cdot f \cdot (dL/Dh) \cdot (dn \cdot V^2/2) = 2 \cdot f \cdot (dL/Dh) \cdot G^2/dn, \qquad [15]$$

pressure loss is calculated and subtracted from total pressure. Based on new pressure and temperature, the interpolation routine calculated toluene properties for the next loop. This process is repeated until the bulk temperature of toluene reached or surpassed 644°K.

Table 6 summarizes a few results. Input variables were the 75 KWe flow rates and geometry of the exchanger heat transfer surfaces. Pressure effects on the mercury were ignored and geometry was varied from the toluene sizing geometry (square passage) to A_C/A_H ratios greater than ten. Fin spacing, thickness, and length were varied to judge their impact on heating length, pressure drop, and unit mass. Output variables were cold and hot side areas, average cold side effectiveness, average toluene heat transfer coefficient, volume of the surfaces and flows, and mass of the heat transfer surfaces.

The values in table 5 were sampled after the lower limit of 0.6 mm was determined for fin thickness and 2.75 mm determined to be the optimum value for fin length. Also, the previously mentioned pessimism in the

incremental change in toluene temperature due to the specific heat interpolation is evident in the detailed heat balance. The result was that mercury quality went to zero approximately 5 cm before the toluene reached 644°K. The configuration with the asterix (*) was selected for further investigation. Fin length and spacing remained the same, but a heating length of 129 cm was obtained with a fin thickness of 0.62 mm, with practically the same mass. The program was reversed and run as a counter flow, which resulted in a heating length of 123 cm. It should be noted that the hot side area for the (*) configuration is the lowest listed in the table. This will result in a mass and exposed area benefit later. Also, the exit pressure is far enough above the design point to allow integration of turns into the toluene flow for multi-pass.

Table 6 - Finned Plate Performance for Detailed Heat Balance

Length (cm)	Mass (kg)	Press (kPa)	Fin Th (mm)	Fin Sp (mm)	Fin Len (mm)	A_{HOT} (m^2)	# Pass
115	1.656	4275	0.6	0.78	2.75	0.102	32
124	1.563	4219	0.6	0.78	2.75	0.096	28
126	1.594	4230	0.6	0.8	2.75	0.099	28
*131	1.538	4193	0.6	0.8	2.75	0.095	26
133	1.568	4205	0.6	0.82	2.75	0.098	26
118	1.705	4243	0.7	0.8	2.75	0.099	28
124	1.664	4206	0.7	0.8	2.75	0.097	26

An important restriction on the mercury flow is evident from the number of toluene passages. With the mercury hydraulic diameter approximated by 2 X the plate spacing, the only parameter required to maintain turbulent conditions in the mercury channel is the total width of the passage.

$$Re = G \cdot Dh/\mu_U = [\dot{m}'/(Sp \cdot W)] \cdot (2 \cdot Sp)/\mu_U$$

$$= 2 \cdot \dot{m}'/(\mu_U \cdot W) > 10{,}000 \qquad [16]$$

For turbulent conditions at the mercury exit, this figure provides a

maximum allowable width of the exchanger.

The best configuration was checked by selectively varying every flow and geometry parameter in the detailed heat balance. Table 7 details the resulting values for parallel and counterflow calculations. Table E1 in Appendix E gives a detailed account of important values along the heating length.

Table 7 - Parallel and Counter Flow Best Configuration

	Parallel Flow	Counter Flow
G (kg/m²-s)	2169	2169
Dh (mm)	1.412	1.412
Fin Th (mm)	0.620	0.620
Fin Sp (mm)	0.800	0.800
Fin Len (mm)	2.750	2.750
Wall Th (mm)	0.300	0.600
# of passages	26	26
Length (cm)	129	123
Exit Press (kPa)	4206	4216
A_C/A_H	4.44	4.44
Mass (kg)	1.511	1.441

The data in table 7 describes the geometry of the heat exchanger in detail, minus turns, heading, and mercury passage spacing/tapering. The wall thickness is based on stress and deflection considerations, which are discussed in chapter 6. Figure 16 shows the details of the toluene flow passages and figure 17 illustrates the basic configuration for the heat transfer surfaces/passages. This geometry results in a four-pass toluene parallel-counter flow arrangement. The first mercury pass is split to flow over the top and bottom toluene flow units, then merged together for the final pass through the center between the two toluene units. Figure 18 shows the dimensions of these units and expected heading for turns, inlets, and exits. The dimensions are 33 cm long, by 7.446 cm wide, by the height dimension which will be calculated in the next section.

MERCURY PRESSURE FIT

The configuration illustrated in figure 17 was selected primarily for simplicity. Other configurations are possible at varying levels of flow complexity, but this is the only one that will allow full advantage to be taken of the mercury width restriction while allowing a turn which is not overly complicated by the two-phase flow. The set up chosen involves identical toluene passages on the "top" and "bottom". The next step is to fit the correct fraction of mercury flow to each portion of the exchanger and dimension the passages so the two can mix in the center section without flow disruption. Henceforth, the "top" section refers to the uppermost mercury passage in figure 17, corresponding to the first two passes (1st half of heat balance model) of toluene, and the "bottom" is the lower one, corresponding to the last two passes of toluene.

By splitting the mercury into two streams when quality is high and merging them in the center passage, maximum advantage is taken of the width restriction for turbulent flow near the exit (low quality range). At high qualities, the mercury flow may be split and still retain bulk turbulence with Re on the order of 100,000.

The purpose of matching the mercury flow conditions is to provide uniform inlet conditions so that the flow can be split with only a valve of the proper dimensions, and to provide equal pressures and velocities at the inlet to the center section. Quality change in each section was calculated from the quality change determined from the detailed heat balance model. The mercury condensation <u>rate</u> for the top section is assumed to be one-half of that corresponding to the first half of toluene flow in the heat balance formulation. The rate for the bottom section is assumed to be one-half that for the last half of toluene flow.

The condensation rates were converted to quality changes based on the percentage of mass flow in each section. Plate spacing was varied to provide each section with identical pressure changes and velocities after one pass and a 180° turn. Hydraulic diameters were calculated based on uniformly tapered channels with a center fin provided for structural support. Later this central fin will be split up and offset to allow flow mixing and to assist with heading in the center section. Table 8 details the final dimensions and flow parameters for the mercury passages. Figure 19 illustrates the passage geometries and figure 20 illustrates the internal heading of the center section. The internal heading is provided to divert the mercury exit flow around the toluene pass from the top to the bottom toluene unit. The heading turn loss for the middle section is already accounted for in table 8.

Table 8 - Mercury Flow Parameters and Passage Dimensions

	Top Section	Bottom Section	Middle Section
Inlet Velocity (m/s)	58.77	59.00	37.54
Inlet Quality	0.852	0.852	0.4212
Exit Velocity (m/s)	38.02	38.08	0.235
Exit Quality	0.358	0.5312	0.0
Mass Flow Rate (kg/s)	0.34736	0.200	0.54736
Net Press Change (kPa)	+0.122	+0.114	+44.7
Inlet Spacing (mm)	12.2	7.0	14.65
Exit Spacing (mm)	7.8	6.65	2.5

Equation 17 summarizes the pressure change correlation used in the above formulation. There is no gravity term and the compressibility of mercury is ignored.

$$-dp/dz = 2 \cdot f_{TP} \cdot G^2 \cdot v_L / Dh \cdot [1 + X \cdot (v_{LV}/v_L)] + G^2 \cdot v_L \cdot (v_{LV}/v_L) \cdot (dX/dz) \quad [17]$$

The first term can be recognized as the normal pressure loss for flow in tubes which is adjusted by a two phase correction factor based on quality.

The two phase friction factor is calculated with a mean viscocity based on quality. The second term is the momentum recovery term. The values in table 8 were calculated using root-mean average conditions from section inlet to outlet with dz as the section length (33 cm).

CHAPTER 5 - DESIGN PERFORMANCE

This chapter presents the performance of the heat exchanger in its final configuration. Sources of possible error in calculations are discussed and detailed fluid and flow parameters are presented in tabulated and graphical form. Off design performance is predicted and transient response during start-up is discussed.

DESIGN POINT PERFORMANCE

Table 9 details the significant flow parameters and fluid properties along the toluene heating length at 11 cm increments. Figures 21-26 graphically represent the significant calculated values. The toluene flow length is measured from the toluene inlet. Just prior to entry, the toluene experiences a 90° turn, and then abrupt contraction as the flow enters the finned channels. At lengths 33, 66, and 99 cm, the flow exits the passages, mixes, goes through a 180° turn and re-enters for the next pass. At length 132 the toluene exits for the last time, goes through a final 90° turn and is ducted to the turbine. All values, including mercury, are given in terms of the local distance (z) from the toluene inlet.

The quality distributions from the detailed heat balance are superimposed on the mercury flow passages. A check comparing the condensation rate to the actual heat transfer rate indicated that these values were so close the values which would be calculated that there was no need to change the assumed distribution. One of the advantages to the toluene multi-pass is that the heat transfer rate gets good distribution throughout the length of the exchanger. Figure 21 shows the value of h_{Hg} along the toluene flow. This value is calculated as the average between

the local value of the outer (top/bottom) and middle sections of the exchanger. The effect of very low quality near the mercury exit is evident in the steep gradient at the beginning, middle, and end of the toluene flow length.

Table 9 - Properties and Flow Parameters Along Heating Length

Length (cm)	Temp (°K)	Press (kPa)	h_{TOL} (W/m²-°K)	E_c	U_H (W/m²-°K)	Q (W)
Inlet	488.7	4440	-	-	-	-
0	488.7	4436	-	-	-	-
11	529.9	4429	8271	0.717	21640	2052
22	559.9	4422	9068	0.700	22760	1634
33	580.4	4415	9813	0.686	23670	1324
Turn	580.4	4412	-	-	-	-
44	592.6	4403	10300	0.677	24540	1135
55	598.4	4391	10310	0.677	24720	1031
66	603.2	4376	16560	0.590	29110	1111
Turn	603.2	4368	-	-	-	-
77	610.5	4350	13440	0.628	29770	980
88	619.2	4327	11120	0.663	26470	703
99	627.7	4301	10450	0.675	25290	509
Turn	627.7	4288	-	-	-	-
110	634.5	4261	10340	0.677	25350	378
121	639.8	4232	10410	0.676	25660	279
132	643.8	4202	10500	0.674	24880	195
Exit	643.8	4211	-	-	-	-

Attention is called to the exit temperature of 643.8°K. There are two reasons the design is not going to be lengthened to force this value to 644.0°K. The first has already been mentioned, and is the small error associated with calculating the temperature change as a function of the interpolated value of specific heat. The error is small, but accounted for a 5 cm difference in the heat balance model length between toluene reaching 644°K and mercury quality going to zero. Two routines were run in the calculations which checked total heat transferred. One was based on summing the total Q and the other on total enthalpy change. Since the calculated value of enthalpy is based on local temperature, it reflected

the "missing" heat transferred to the toluene. Total Q is based on the flow parameters along the length and indicated that 137.46 KW of thermal power had been transferred by the end of the heating length, exactly the base cycle requirement.

The other reason for not changing the design is the pressure loss. The reference cycle assumed a pressure drop of 10.4% through the heater. The actual drop here is 5.4%. Without considering the effect on the regenerator, this will result in pump power savings which will be realized in shaft output to the alternator. A preliminary estimate on the savings indicates that the required enthalpy change across the turbine to produce the reference cycle shaft power at the same mass flow rate is 2719 J/kg less than that required in the reference cycle. Adjustments to the reference cycle are recommended in chapter 7. The savings are pointed out here to indicate that the heat exchanger delivers the required performance to operate the cycle at the design point.

Figure 22 plots the toluene temperature along the flow length. Figure 23 plots the pressure change from inlet to outlet. The steps in the plot represent the turn losses within the exchanger. Figures 24 - 26 show h_{TOL}, U_H, and total Q respectively. The apparent discontinuity in h_{TOL} and U_H (figures 24 and 25) do not really exist. The jump occurs when the bulk fluid temperature goes above the specific heat spike and heat transfer correlations are switched. Shiralka [12] demonstrated that the full value for the heat transfer coefficient is reached by the time the bulk temperature reaches the T_{CRIT}. A smooth curve was not superimposed because it is uncertain if toluene correlates the experimental data of the test fluids. This provides a degree of confidence in the present rate of heat transfer.

Reference the amount of heat transferred in figure 26, it is noted that 98% of the required heat transfer occurs in the first 90% of heating length (119 cm). The last 5°K of temperature accounts for approximately 2.3% of the heat transfer and uses 10% of the heating length (mass). The impact of changing the peak toluene temperature will be discussed in chapter 7.

RADIATION LOSSES

The radiation losses from the external surfaces of the unit were calculated for the final external dimensions. The estimate evaluated an uninsulated molybdenum surface radiating at 654 °K into a background at 250 °K. This results in a radiation loss of 32 watts. When account is taken of system configuration and view factors with other components, the estimated loss is less than 20 watts (0.015% of heat transferred). Radiation effects were therefore neglected.

OFF DESIGN PERFORMANCE

The heat exchanger was evaluated for performance at the 50 KWe power level. It is noted that the mercury exit dimensions (spacing = 2.5mm) was set for the critical diameter corresponding to the 50 KW level since the design goal was to ensure efficient operation over the range 50-75 KWe. The heat balance indicated complete mercury condensation at 97 cm flow length. Running these values through the exchanger, the mercury will sub-cool to approximately 647°K and the toluene will superheat to approximately 645.5°K. Toluene exit pressure is 4286 kPa.

If the exchanger is operated at mass rates in excess of 75KWe, the main effects are lower toluene temperature, and greater pressure loss. At a 90 KW power level, the toluene temperature reached 637°K, which means

that mercury condensation was incomplete. Exit pressure was 4071 kPa. This does not mean the unit will not operate at higher power levels. However, if it is desired to do so, the mercury flow rate cannot be increased in proportion to the toluene rate. If all units of a configuration such as figure 6 were operating through the exchanger, power output is estimated at approximately 90 KWe since the mercury mass rate will be reduced and the toluene enthalpy change will not be the reference cycle value.

Operation below 50 KWe is uncertain. Since the mercury passages were dimensioned for known critical values, operating at a lower mass rate will likely produce unfavorable two-phase flow effects. Since the vapor velocity will be reduced, droplet entrainment may be degraded, reducing h_{HG}. This will probably be offset by the much shorter heating length required by the toluene at a lower mass rate. However, the mercury exit is dimensioned to prevent slug flow at mass rates above the 46 KWe power level (4 KW safety factor on vapor We number). Flow instabilities may result below this level.

TRANSIENTS DURING START-UP

One of the concerns about the toluene multi-pass is the possibility of two-phase flow problems arising from liquid being centrifuged to the outer passages after a turn, as indicated in figure 27. The following discussion assumes that the starter/generator can motor the pumps to 10% of the full operating mass rate (provide a G = 216.9 kg/m^2-s). The shape of the saturated vapor line on the T-S diagram indicates that toluene is a friendly material in dealing with this sort of problem. As saturated vapor leaves the boiler and passes through the ducting and turbine, its expansion will be dry. Since little energy will be extracted from the

flow during start-up, this expanding vapor will be able to evaporate residual liquid in the ducting and turbines.

Within the condenser/boiler the flow will probably separate into the two phases. This will be shown not to present a problem, as complete vaporization should occur well before exit. Experimental data of Kays and London [28] show that, for a plate-fin exchanger with almost identical passage dimensions as the present exchanger, transition from laminar to turbulent flow parameters will begin at Reynolds numbers around 250 and will achieve fully turbulent conditions at Re of about 5000. The following comparison will use pessimistic turbulent values since toluene flowing at 10% of the full mass rate at a cold start-up will have an initial Re of about 760. Nucleation effects (which enhance heat transfer) are neglected.

Recall the trend in the toluene sizing where lowering mass velocities significantly decreased heating lengths. Using Rohsenow's form of dimensional analysis [30], $h_{ST}/h_{SS} = 0.25$, which implies incremental $Q_{ST}/Q_{SS} = 0.25$ (toluene dominating). Using $Q = m' \cdot Cp \cdot \Delta T$, then $0.25 = (0.1) \cdot (0.8) \cdot (\Delta T_{ST}/\Delta T_{SS})$. This indicates that the incremental rate of toluene temperature change per unit of heating length during start is approximately three times that during steady state operation. This means that boiling length will be much less than the total length of flow. Of course, as the toluene is heated and becomes fully turbulent, the h_{ST} will go up dramatically, further enhancing boiling. Also, pressure drop will be more significant in the vapor flow due to its lower density and higher velocity. This will more than offset the higher friction factor associated with the liquid flow and will ensure that the liquid flow does not become choked.

Response time to eliminate all liquid will depend on the length and geometry of ducting and plumbing associated with the turbine. Residence time for a toluene particle in the exchanger will range from 0.5 to 4.0 seconds during depending on boiling length. The liquid concentrations in other components will be exposed to a "dry" environment very quickly. Based on the above estimate, recommend increasing the pumping rate as soon as the turbine is dry. In this manner, the heating process will go supercritical as soon as the turbine begins producing shaft power.

CHAPTER 6 - MATERIALS AND ASSEMBLY

This chapter summarizes the material selection criteria and indicates reasons for rejecting certain materials. Dimensions are determined for the outer shell based on strength and impact risks from micrometeoroids. Stresses on internal components are determined and presented in terms of yield strengths. Possible assembly and construction techniques are introduced and recommended based on reliability.

MATERIAL SELECTION

The criteria used in chapter 3 to select molybdenum as the heat transfer surface is the dominating criteria, given other material conditions have been met. These other conditions are corrosion resistance in a mercury environment, good strength, and workable properties. Other candidate materials are tantalum, niobium, and advanced alloys. As indicated in chapter 3, the heat transfer characteristics of steel based alloys were not competitive with molybdenum.

Tantalum has a density higher than molybdenum (16,600 kg/m^3) and a thermal conductivity of about 63 $W/m\text{-}^oK$ in the temperature range of interest [16]. Compared with molybdenum these properties would make the unit more massive and give it a larger cube. Its strength and other material properties are comparable to molybdenum and would provide an excellent alternative to using steel based alloys.

Niobium is probably the second best candidate. Its density is 8570 kg/m^3 and thermal conductivity in the range of interest is 60 $W/m\text{-}^oK$. Niobium was eliminated from consideration due to its long term creep behavior [16]. Niobium has measurable creep at elevated pressures over a wide range of temperatures, including the temperature range of the current

unit. The walls of the passages will have to withstand 4.45 MPa applied to the fins, which will impose tension stresses of 41 MPa on the average wall cross section (of 0.30mm). Under these loads, Niobium has measurable creep in 1000 hour testing, which would required thicker dimensions.

Molybdenum has measurable creep only in temperature ranges above the condenser/boiler (over 800°K) at pressures over 250 MPa. The modulus of elasticity at 654°K is 290 GPa, the 0.01% yield is 170 MPa, and the tensile strength is 260 MPa. Additionally, long term corrosion tests with mercury at elevated temperatures (over 600°K) indicated no measurable deterioration [31].

PLATE DIMENSIONS

Up to this point, the dimensions of the surfaces have been determined by heat transfer considerations. As indicated earlier, the wall thickness of 0.30 mm was based on deflection stress imposed by the internal fluid stresses at 4450 kPa. The model used assumed a clamped beam with the load applied in the center (for pessimism). The maximum deflection calculated was $6X10^{-8}$ meters, which is very small [32]. However, the tension and compression stresses at the surfaces is 25 MPa. If the previous value of 0.20 mm had been retained, the deflection would have been approximately twice as much with stress on the order of 43 MPa. This combined with the tension stress imposed by the fluid outward on the fins would put the combined stress over 100 MPa, too close to the 0.01% yield point. With 0.30 mm thickness, the maximum stress in the center of each passage is approximately 66 MPa, less than one-half of yield.

Two parameters must be considered when determining the thickness of the outer packaging for the unit, deflection stresses and threat of micrometeoroid penetration. Both values were calculated and the most

pessimistic used. Using a penetration equation which relates penetration depth to material densities, mass and velocity of impacting material [33,34], penetration depth is calculated based on target material thickness. Using published data on micrometeoroid population [35], the probability of penetration is calculated as a function of exposed surface area and time. The exterior dimensions of the heat exchanger were used, and the time scale calculated for a 0.9 probability of no penetrations in 7 years. This gives a size scale to the threat and plate thickness is scaled up by a factor of 1.5 to ensure no penetration. This analysis gave an exterior thickness of 0.32 mm for a probability of 0.9 of no penetration of a molybdenum surface in 7 years.

The deflection stress was calculated using the width of the exchanger, 7.34 cm, with the load being the static pressure of mercury on the plate. To add a safety factor, the ends were assumed pinned, and the maximum allowable stress was set at 85 MPa (50% yield). This gave a thickness value of 0.90 mm. Since this is the most pessimistic value, it will be used.

DUCTING AND HEADING

The internal passages for the toluene turns will be made the same thickness as the toluene passage walls, 0.30 mm, since they need to contain the same pressure as the toluene passages. Externally exposed ducting will use a thickness of 0.50 mm to provide a safety factor above the penetration criteria. The side plates will also be a thickness of 0.50 mm (figure 28).

The toluene turn passages will be configured to provide a cross section proportioned to keep the mass velocity constant from the exit of one pass to the entrance of the next (figure 29).

Recall that the mercury dimension calculations allowed for a central fin to provide structural support and assist with internal ducting. This fin is split into 2 cm sections and offset 1 cm from the centerline at intervals of 1 cm to allow complete mixing of the mercury flow (fig. 20).

JOINING AND WELDING

There are several processes available which might satisfactorily join the pieces of the exchanger together. Given the cost of system delivery to the space station and the desirability of high reliability, Eagar [36] recommends using a diffusion bonding process to attach the fins to the plates. With this method, no materials are used other than the molybdenum surfaces and the end product will have the characteristics that cutting the unit out of a solid block would have provided - near perfect seams where the fins join the plate and no material disruption due to a welding process. This process is the most reliable since care in setting up the furnace and pressure equipment will ensure complete bonding. The disadvantage to this process is cost. Very likely, a special furnace will have to be built to handle the pressures and temperatures to bond molybdenum. Eagar points out that this process is particularly suited to fabricating units where dimensions are small and inspection will be difficult.

A less expensive alternative, but almost as reliable as diffusion bonding is transient liquid phase diffusion bonding. This is a brazing type process where another material, with lower melting temperature than molybdenum, is vapor deposited on the ends of the fins. Then the unit is pressurized and heated to near the melting point of the deposited material and slowly cooled. There are two restrictions on this process for the present case. The first is mercury compatibility of the bonding material.

The second is selecting a material which will not form an alloy with molybdenum during the bonding process.

Alternative approaches involve laser or electron beam fusion welding. While these are not as desirable for the plate-fin arrangement, they are probably best suited for attaching the external plates and ducting. Redundancy and reliability can be enhanced by first fusion welding, then brazing or welding another, foil thin, section over the first weld [37].

Since reliability is a major concern the recommended process is to diffusion bond the plate-fin surfaces and as many other elements as possible. Probably the first and third internal toluene turns could also be diffusion bonded. The other surfaces and ducting will likely need to be welded or brazed in place.

CHAPTER 7 - CONCLUSIONS AND RECOMMENDATIONS

DISCUSSION

The final exterior dimensions of the condenser/boiler are illustrated in figure 30. The total mass is 2.251 kilograms including toluene inlet and outlet, but not including the mercury inlet and outlet. Total cube is 0.0012 m^3 and estimated delivery cost is $5390, of which $4963 is mass cost. The unit has a heat transfer effectiveness of 0.94 based on temperature and 0.96 based on enthalpy changes (heat transferred). The mass performance is 0.016 kg/KWth.

The design configuration is considered within the constraints of the required performance because the heat transfer coefficients are conservative. Shiralkar's tests indicated that full fluid heat transfer returned before the bulk temperature reaches the specific heat spike. The large step indicated in figure 24 would should be a smooth curve, with enhanced heat transfer in the toluene mid-range and shortening heating length. The average mercury heat transfer coefficient is about 32,000 Btu/hr-ft^2-^oF. This is near the lower end of the SNAP-8 test data (22,000 - 147,000 Btu/hr-ft^2-^oF).

The location of the specific heat spike may be cause for concern. The model presented here evaluated the heat transfer based on known ranges of validity for the heat transfer correlations. The curve in figure 24 was not smoothed out because toluene test data is apparently not available in this range. This region of uncertainty in heat transfer occurs in the exchanger where the middle section mercury quality is near zero. Accurate test data for toluene in this specific temperature range might alleviate this concern by moving the peak heat transfer range to a different location in the exchanger (reducing heating length).

One note of caution is offered concerning predicting toluene heat transfer with the Swenson correlation. If extended surfaces are employed the T_{WALL} used should be an adjusted value based on the average wall temperature the fluid experiences, not the fluid temperature at the fin base. If the latter is used, the resulting lower viscocity value will give too high a value to Re_w, providing too high a heat transfer coefficient.

The favorable pressure drop in the heater means that the turbine will need to provide less pumping power then expected. It is also possible that the regenerator pressure loss will not be as high as expected. If the power output of the system is to be maintained at 75 KWe, the toluene and the mercury mass flow rates need to be adjusted down slightly.

As previously indicated, 10% of the heat transfer surface is dedicated to transferring 2.3% of the heat to the toluene. The effect of changing the pinch temperature difference by 5°K would reduce the mass of the unit by approximately 8%. The mass flow rate of toluene would have to increase by 2.2% to maintain thermal equilibrium and deliver the required power. The effect of adding one more toluene passage to accomodate a slightly increased flow rate would only add 3.4% to the mass. Of course, every other component will be affected also. The net savings of one tenth of a kilogram in the heater would have to be balanced against possible mass gains in the other components. It is likely that greater mass savings can be achieved at the bottom of the cycle if temperatures within the cycle are kept at maximum values.

The only recommended change involves correcting for the pump power in the toluene cycle. The peak cycle pressure should be set at 4.99 MPa at pump outlet. The mass flow rates are adjusted down by 0.22% each. The net effect is a system efficiency of 0.412 (up from 0.411).

CONCLUSIONS

A very compact, lightweight heat exchanger can be constructed with materials and techniques currently available. In light of system considerations, there is probably no advantage to be gained by reducing the mass of the unit further. Any changes in operating conditions should be based on considerations of other system components. Further research and component development is considered unnecessary provided the uncertainties in heat transfer can be alleviated.

RECOMMENDATIONS

To resolve the uncertainties in heat transfer coefficients, experiments need to be conducted with supercritical toluene and condensing mercury. The correlation used for mercury fit the available data, but is simplistic and doubtlessly incorrect. Mercury needs to be investigated for trends associated with variable passage geometry to determine the effects of flow acceleration. Toluene needs to be investigated for its compatibility with one or the other heat transfer correlations, or a different one. Specifically, its supercritical behavior within +/- 50°K of the specific heat spike needs to be verified.

If tests indicate that mercury performance is worse than predicted, or toluene is as poor as predicted here, then the geometry of the current design should be modified to move the critical values away from each other (away from the mercury liquid exit). Any other test result will improve the performance of the exchanger, moving the current range of uncertainty away from the mercury exit, reducing the exchanger's total length.

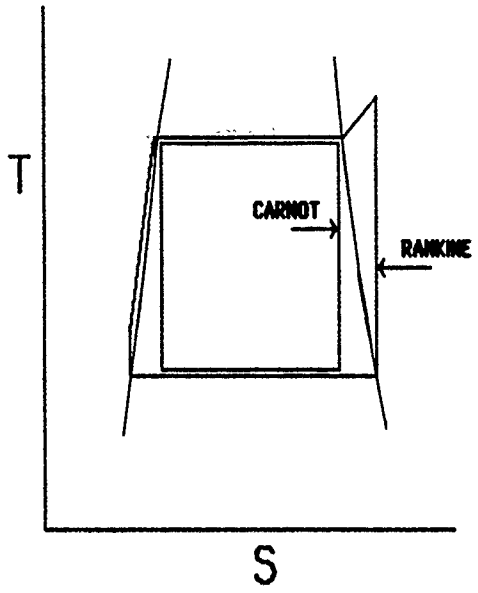

Figure 1 - Rankine and Carnot Cycles on Temperature-Entropy Diagram

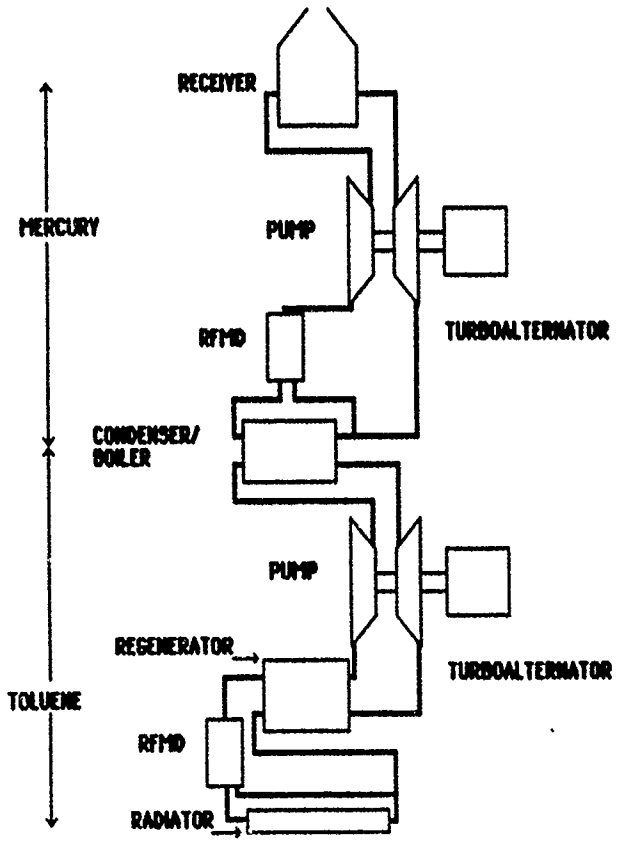

Figure 2 - Binary Cycle Schematic

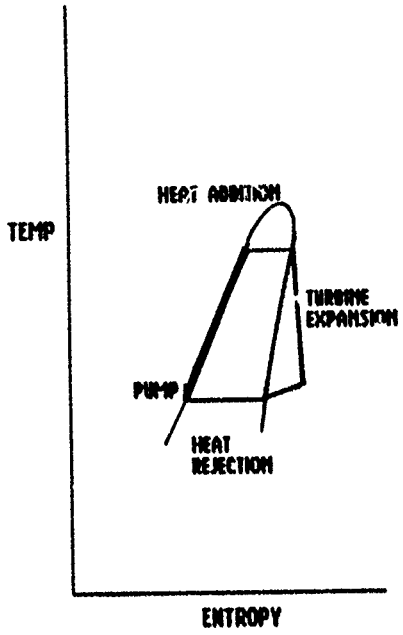

Figure 3 - Organic Rankine Cycle

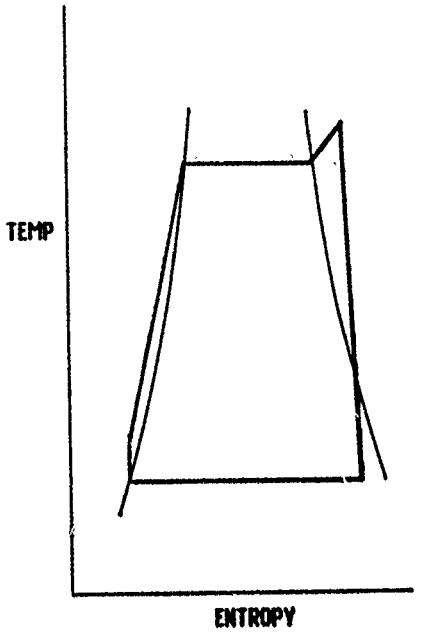

Figure 4 - Mercury Rankine Cycle with Superheat

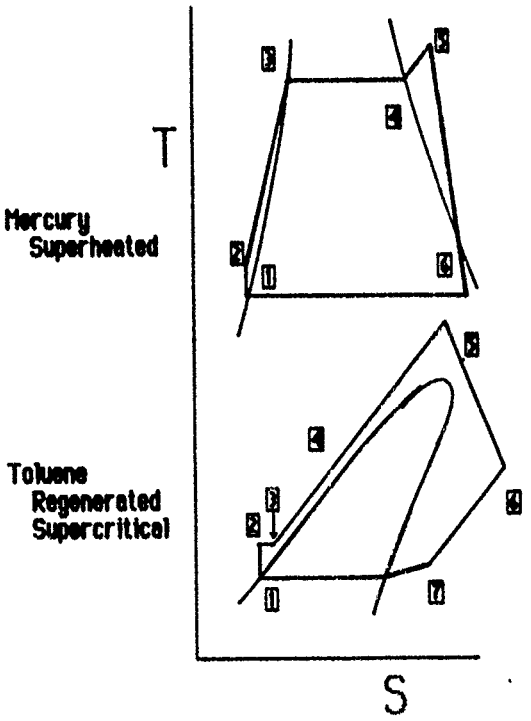

Figure 5 - Combined Cycle T-S Diagram

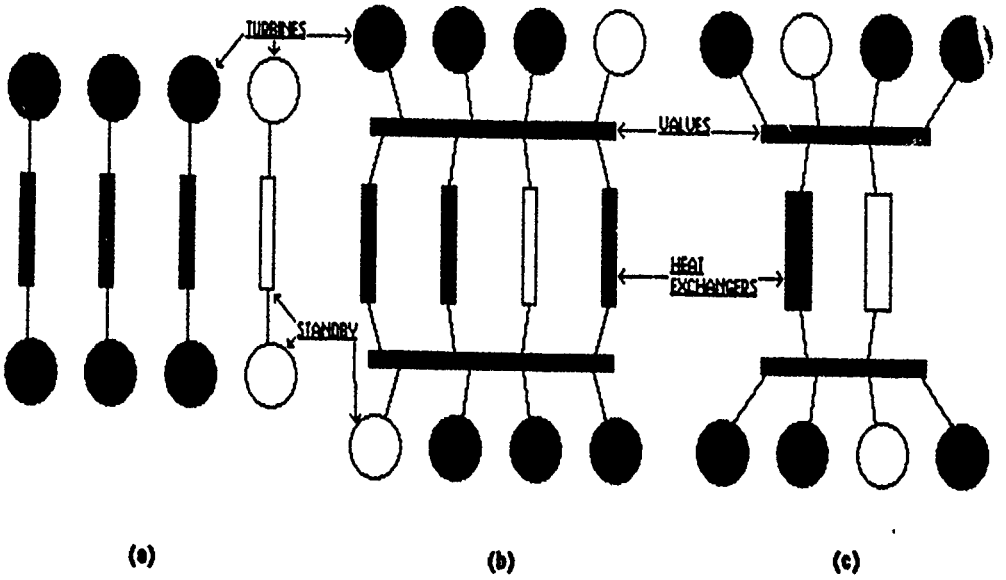

Figure 6 - Heat Exchanger Configurations

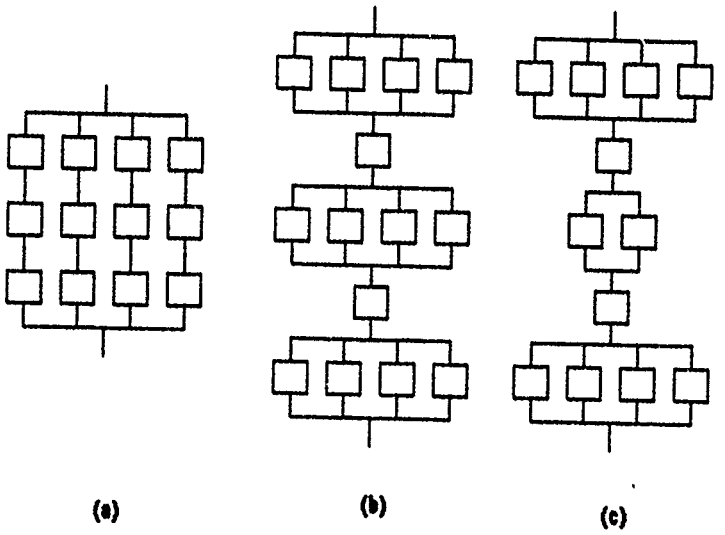

Figure 7 - Reliability Networks for Figure 6

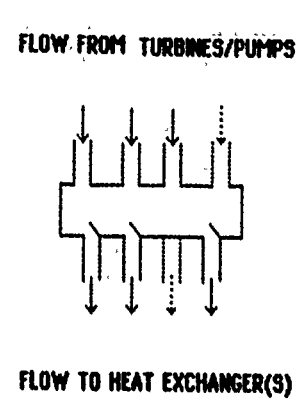

Figure 8 - Reliability Model for Valves

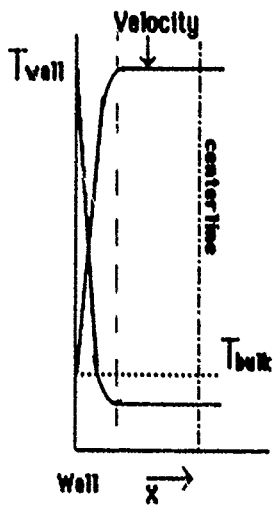

Figure 9 - Turbulent Velocity and Temp Profiles

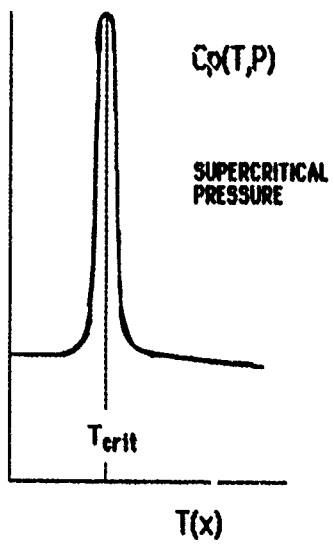

Figure 10 - Specific Heat Spike in a Supercritical Fluid

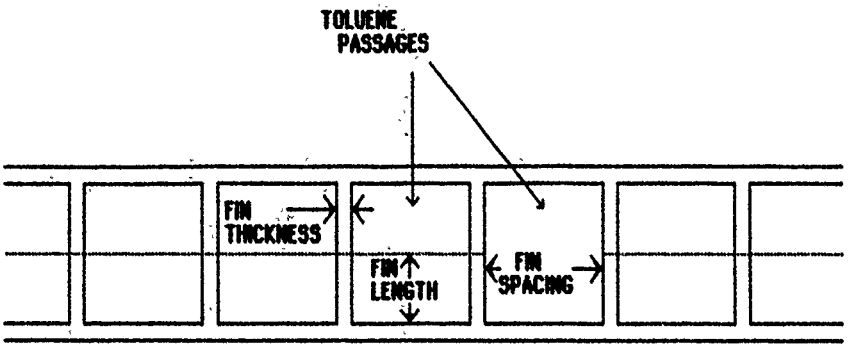

Figure 11 - Toluene Passage Sizing Model

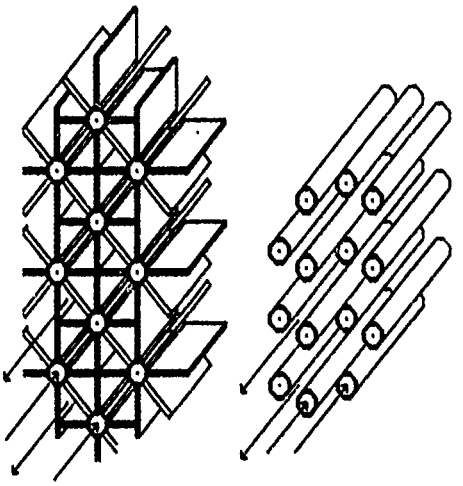

Figure 12 - Finned and Unfinned
Tube Bundles in Counterflow

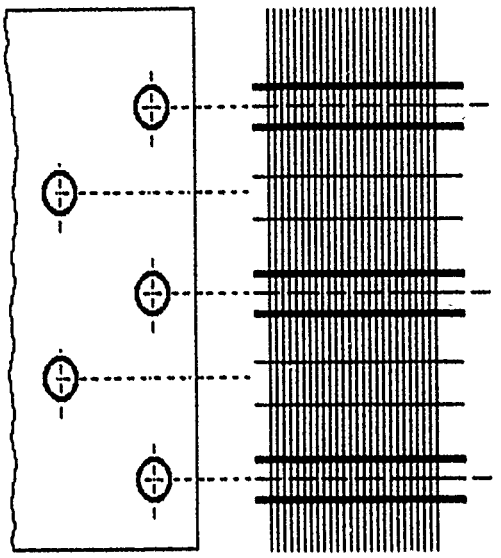

Figure 13 - Finned Tube Cross Flow

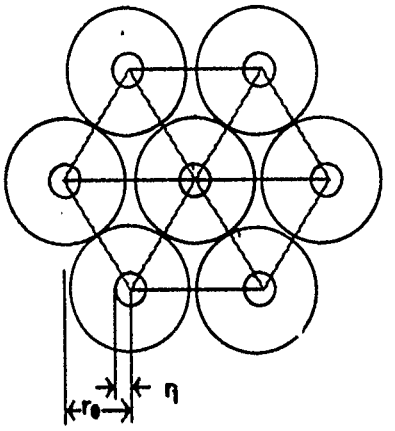

Figure 14 - Circular Fin Model for Figure 13

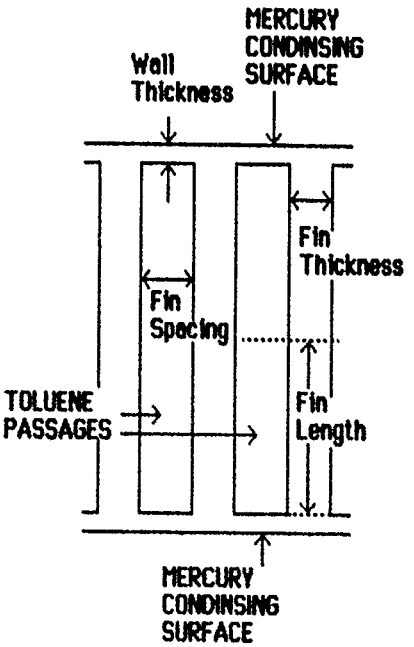

Figure 15 - Plate - Fin Configuration

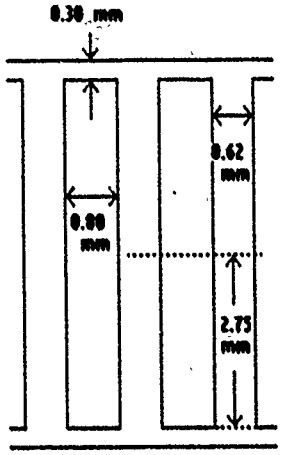

Figure 16 - Toluene and Heat Transfer Passage Dimensions

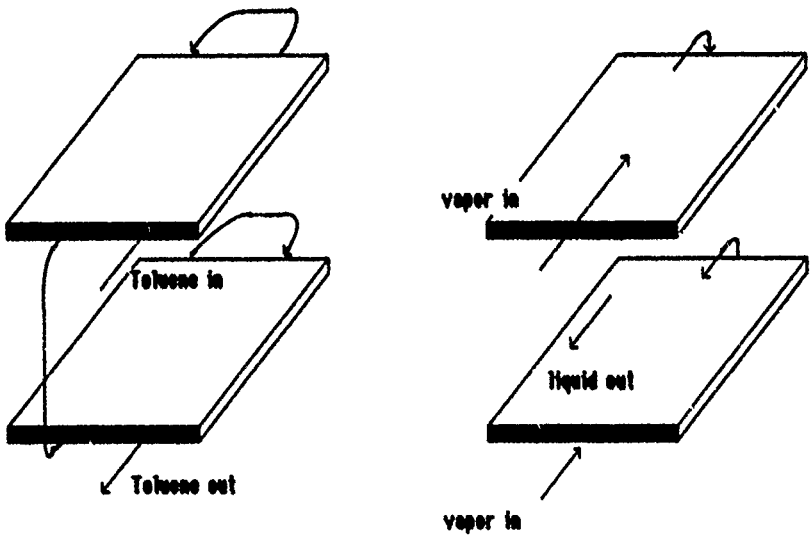

Figure 17 - Fluid Flow Patterns

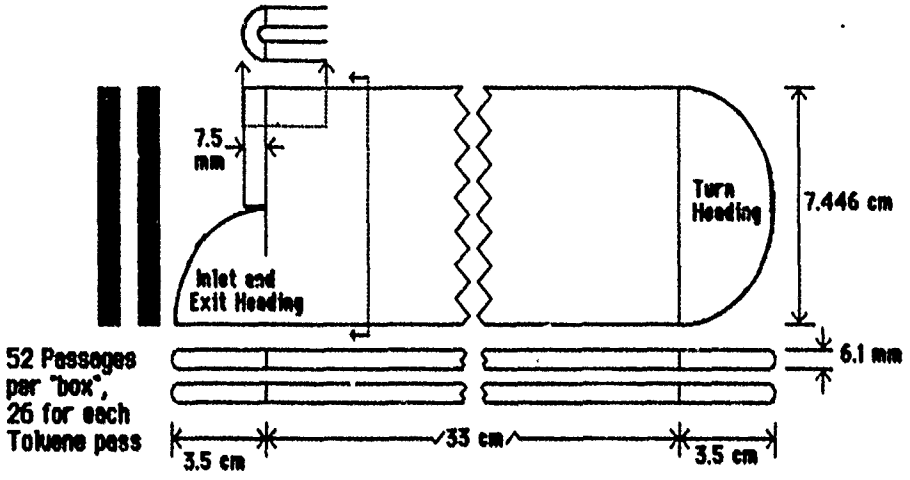

Figure 18 - Toluene Passage Dimensions and Heading

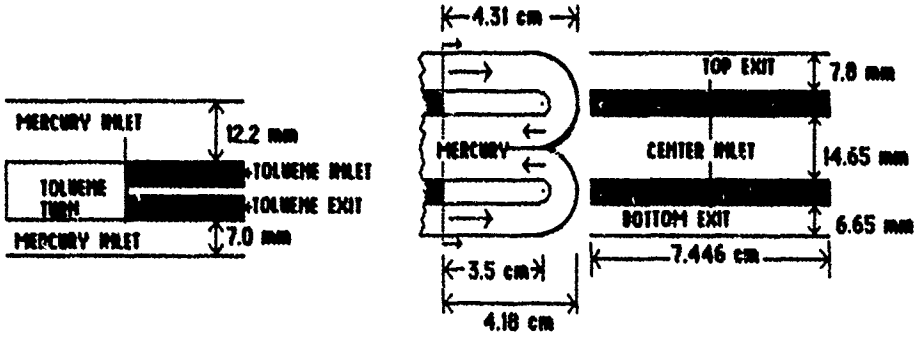

Figure 19 - Mercury Passage Dimensions

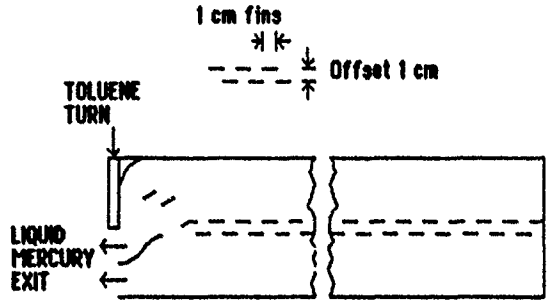

Figure 20 - Mercury Heading in Center Section

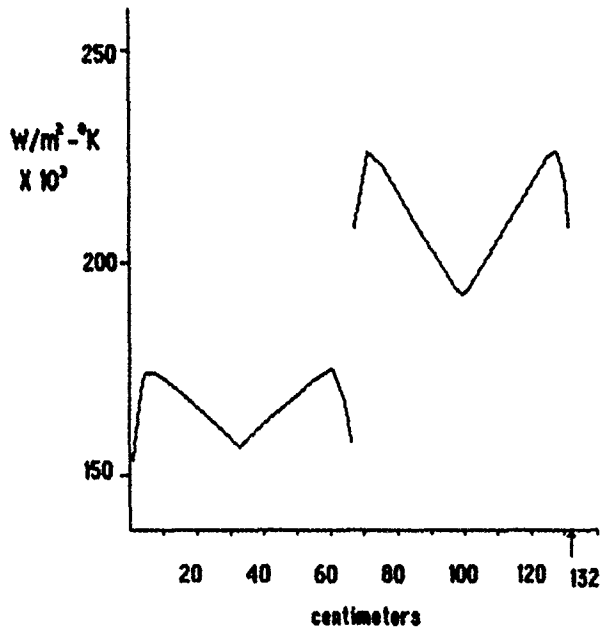

Figure 21 - Mercury Heat Transfer Coefficient (average)

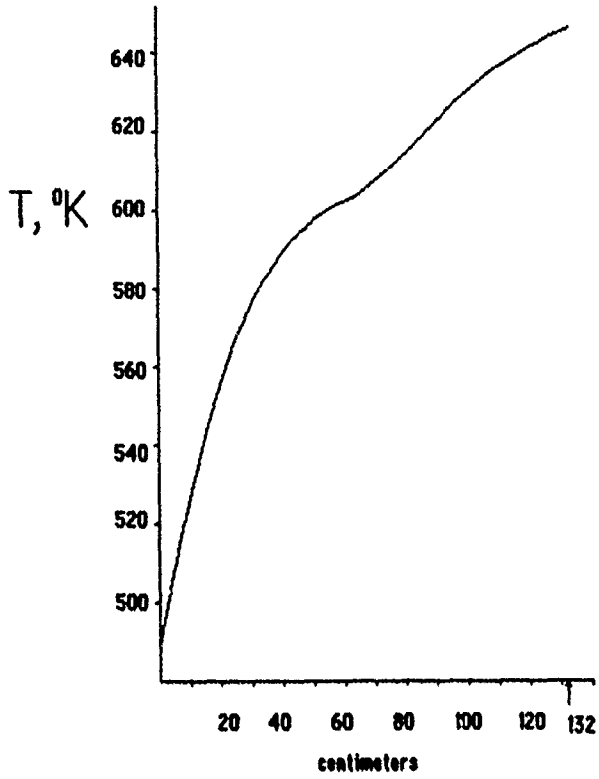

Figure 22 - Temperature Along Toluene Flow Length

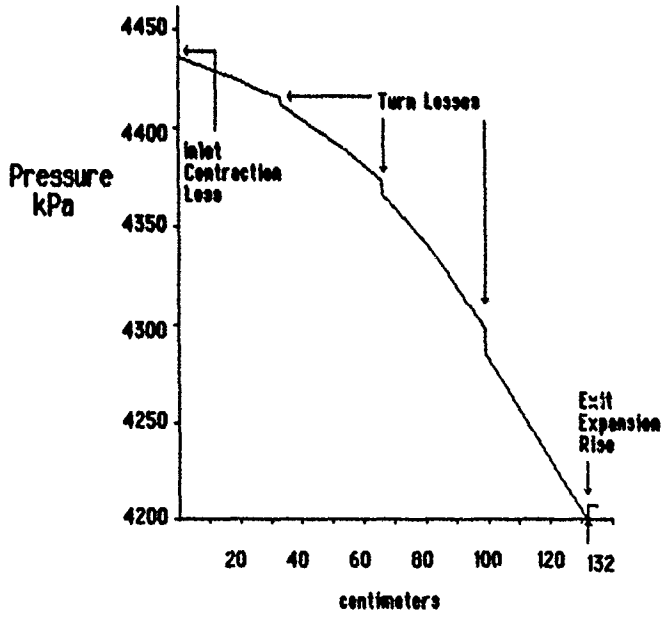

Figure 23 - Toluene Pressure Loss

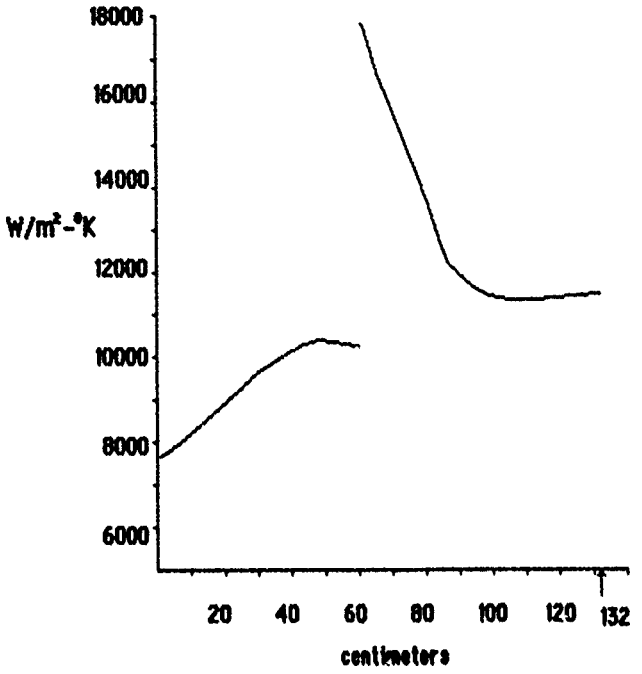

Figure 24 - Toluene Heat Transfer Coefficient

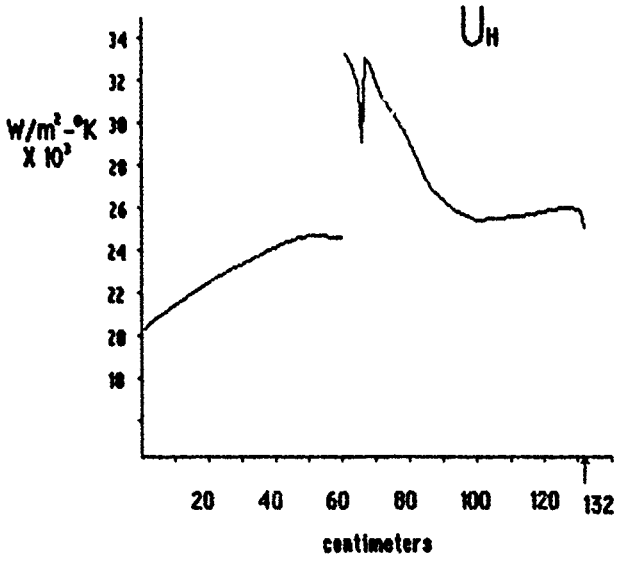

Figure 25 - Overall Heat Transfer Coefficient

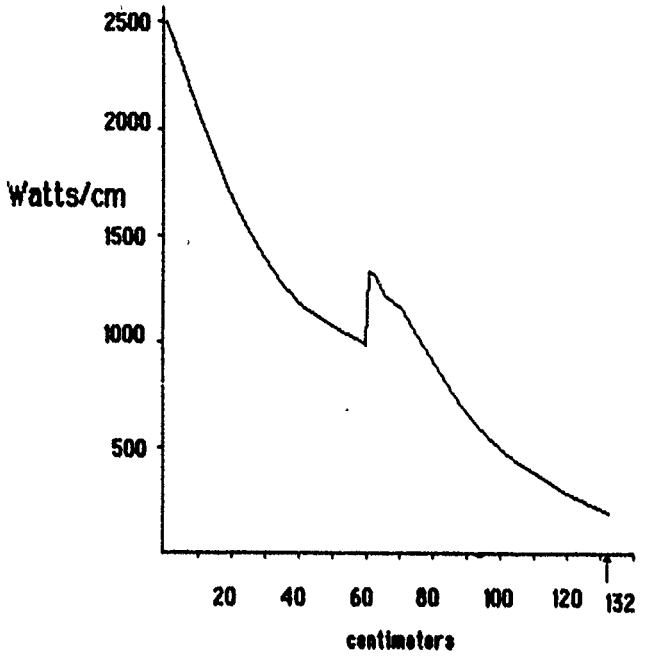

Figure 26 - Heat Transfer Rate

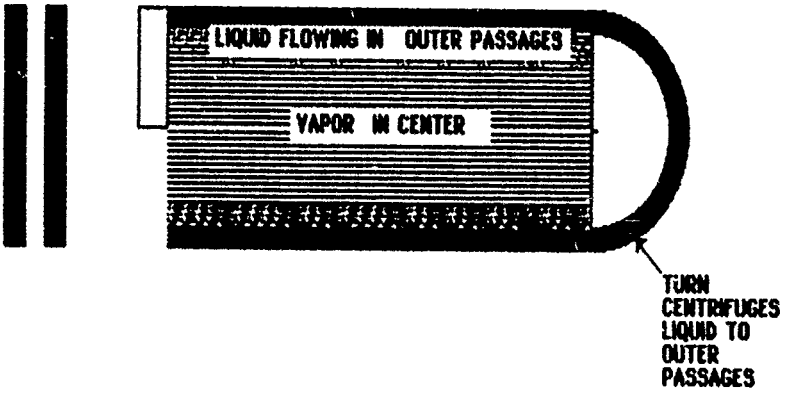

Figure 27 - Transient Two-Phase Flow

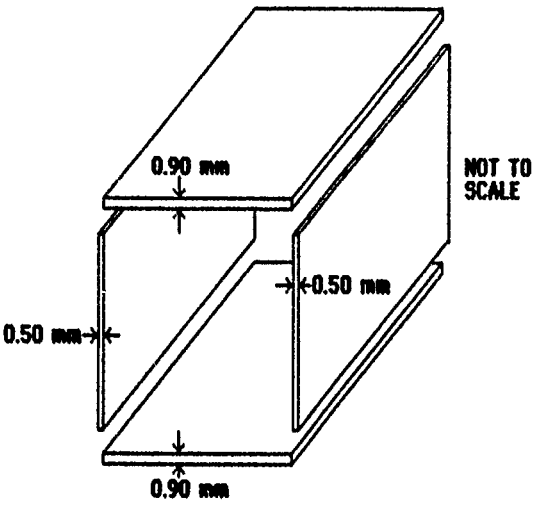

Figure 28 - Outer Plate Thicknesses

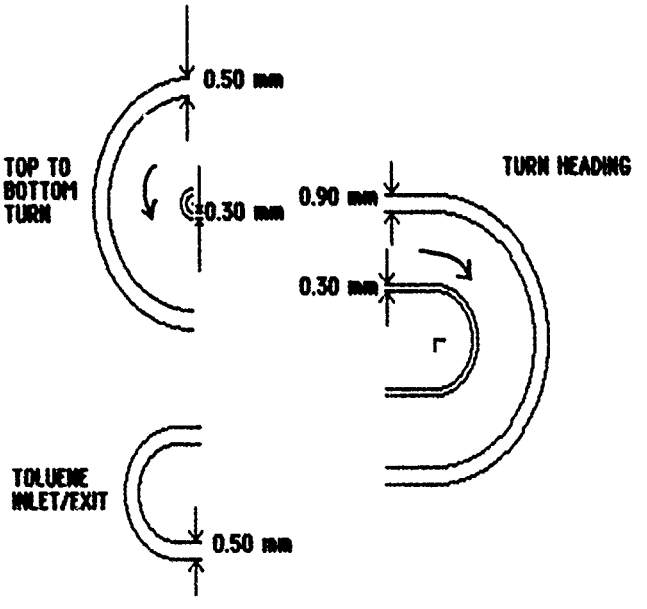

Figure 29 - Heading Wall Thicknesses

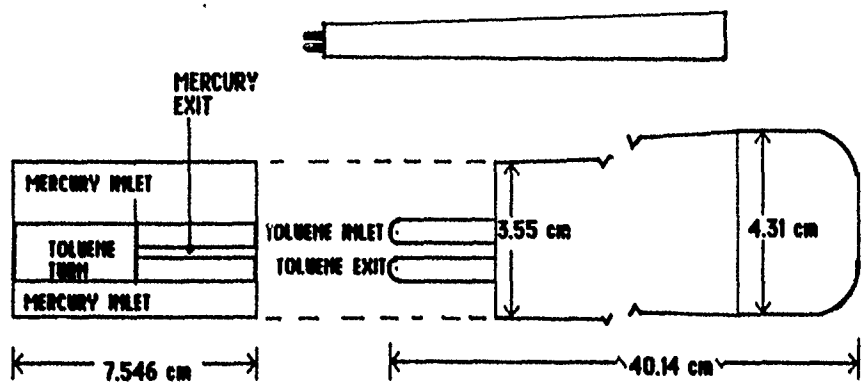

Figure 30 - Exterior Sketch

APPENDIX A - TOLUENE PROPERTY TABLES

The tables in this appendix detail the significant properties of toluene for the range of temperatures and pressures for the condenser-boiler. The data was provided by Sunstrand [38] and matches well with other sources [39,40], but is much more detailed. The linear profile assumed in the initial sizing was determined by interpolating the tabulated values in a straight line from the inlet temperature and pressure to the exit condition of the reference cycle. For all subsequent calculations, the values were integrated into a computer subroutine to calculate the properties at every calculation loop.

The fluid thermal conductivity and viscosity are liquid and vapor values which have been adjusted for the supercritical pressure. In the range of the current problem, they may be considered functions of temperature only.

Table A1 - Toluene Specific Heat (J/kg-°K)

	Pressure (kPa)			
Temp (°K)	4137.41	4309.80	4482.19	4654.59
488.71	2383.81	2382.14	2380.05	2377.95
494.26	2401.82	2399.72	2397.63	2395.54
499.82	2422.33	2420.24	2417.72	2415.21
505.37	2444.52	2442.01	2439.08	2436.56
510.93	2467.54	2464.61	2461.68	2458.75
516.48	2493.92	2490.57	2487.22	2483.87
522.04	2523.22	2519.46	2515.27	2511.08
527.59	2555.88	2551.27	2546.67	2542.06
533.15	2593.56	2588.12	2582.67	2577.23
538.71	2637.52	2631.24	2624.54	2617.84
544.26	2693.20	2685.66	2677.71	2669.75
549.82	2755.16	2745.53	2735.90	2726.27
555.37	2835.54	2823.40	2810.84	2798.70
560.93	2936.02	2920.11	2903.78	2887.45
566.48	3065.80	3044.03	3022.26	3000.49
572.04	3249.59	3218.19	3186.79	3155.39
577.59	3513.34	3463.94	3413.12	3364.72
583.15	3955.44	3867.52	3779.60	3691.69
588.71	4997.89	4696.87	4395.86	4262.73
594.26	20592.31	7993.77	7242.71	6663.71
599.82	4381.21	14587.56	7535.76	5990.09
605.37	3379.37	5980.88	8582.40	7674.34
610.93	3051.98	4770.56	6489.13	6928.30
616.48	2880.75	3509.99	4139.23	4768.46
622.04	2777.77	3077.52	3377.28	3677.03
627.59	2709.11	2887.87	3066.64	3245.40
633.15	2660.54	2782.79	2905.04	3027.28
638.71	2625.79	2715.81	2805.82	2895.83
644.26	2600.68	2670.59	2740.51	2810.42
649.82	2581.00	2637.94	2694.45	2750.97

Table A2 - Toluene Density (kg/m^3)

Temp (°K)	Pressure (kPa) 4137.4	4206.4	4275.3	4344.3	4413.2	4482.2	4551.2	4620.1
488.71	660.24	660.48	660.72	660.96	661.02	661.44	661.68	661.92
494.26	652.83	653.09	653.35	653.60	653.86	654.12	654.38	654.63
499.82	645.18	645.46	645.73	646.01	646.29	646.57	646.85	647.12
505.37	637.70	638.00	638.30	638.60	638.90	639.20	639.49	639.78
510.93	629.38	629.71	630.04	630.37	630.70	631.03	631.35	631.67
516.48	621.28	621.64	622.00	622.35	622.70	623.06	623.41	623.75
522.04	612.73	613.12	613.51	613.90	614.29	614.68	615.06	615.44
527.59	603.77	604.20	604.63	605.06	605.49	605.92	606.34	606.76
533.15	595.07	595.54	596.00	596.47	596.94	597.41	597.87	598.32
538.71	584.85	585.38	585.92	586.45	586.99	587.53	588.04	588.55
544.26	574.98	575.57	576.17	576.77	577.37	577.96	578.53	579.10
549.82	564.09	564.78	565.46	566.14	566.83	567.52	568.16	568.81
555.37	552.33	553.12	553.91	554.71	555.51	556.31	557.05	557.79
560.93	541.04	541.93	542.82	543.73	544.62	545.53	546.36	547.20
566.48	525.56	526.71	527.86	529.02	530.18	531.35	532.38	533.42
572.04	510.84	512.31	513.70	515.09	516.49	517.89	519.10	520.32
577.59	490.48	492.51	494.55	496.61	498.69	500.79	502.39	504.00
583.15	465.62	468.58	471.58	474.62	477.69	480.81	482.95	485.12
588.71	443.16	446.87	450.64	454.48	458.39	462.36	464.96	467.60
594.26	248.57	265.58	285.10	307.70	334.20	365.70	378.32	391.84
599.82	172.73	188.94	208.50	232.59	262.96	302.46	318.89	337.21
605.37	152.91	156.88	171.75	189.75	211.95	240.05	254.27	270.28
610.93	134.51	142.65	151.84	162.29	174.29	188.20	198.64	210.30
616.48	125.91	130.79	136.06	141.77	147.99	154.77	162.98	172.10
622.04	120.43	124.66	129.20	134.08	139.34	145.04	151.46	158.48
627.59	115.41	119.08	123.00	127.18	131.65	136.46	141.47	146.86
633.15	111.15	114.43	117.91	121.60	125.53	129.72	133.87	138.30
638.71	107.54	110.54	113.72	117.08	120.65	124.45	128.12	132.02
644.26	104.15	106.91	109.82	112.89	116.14	119.58	122.84	126.82
649.82	101.32	103.91	106.63	109.50	112.54	115.74	118.74	121.91
655.37	98.64	101.07	103.63	106.31	109.15	112.13	114.91	117.83

Table A3 - Toluene Enthalpy (J/kg)

	Pressure (kPa)							
Temp (°K)	4137.4	4206.4	4275.3	4344.3	4413.2	4482.2	4551.2	4620.1
488.71	2531	2534	2538	2541	2544	2548	2552	2557
494.26	15825	15824	15822	15821	15820	15818	15818	15818
499.82	29257	29250	29243	29236	29230	29223	29218	29214
505.37	42688	42676	42664	42652	42640	42628	42618	42608
510.93	56436	56417	56398	56378	56359	56340	56323	56306
516.48	70184	70158	70131	70104	70078	70051	70028	70004
522.04	84136	84101	84065	84030	83995	83959	83927	83895
527.59	98292	98246	98201	98155	98109	98063	98022	97980
533.15	112448	112391	112336	112280	112223	112167	112116	112065
538.71	127187	127115	127042	126970	126898	126825	126760	126694
544.26	141926	141838	141749	141660	141572	141484	141403	141323
549.82	157123	157012	156902	156791	156680	156569	156470	156371
555.37	172778	172639	172500	172361	172222	172082	171959	171835
560.93	188434	188266	188098	187931	187763	187596	187448	187300
566.48	205761	205531	205300	205071	204841	204611	204415	204219
572.04	223087	222795	222503	222210	221918	221625	221382	221138
577.59	242590	242144	241698	241251	240805	240359	240022	239685
583.15	264268	263577	262885	262193	261502	260810	260335	259859
588.71	285946	285009	284072	283135	282199	281261	280647	280034
594.26	347468	342441	337413	332385	327357	322330	319132	315935
599.82	408991	399872	390753	381635	372516	363398	357617	351836
605.37	448516	438976	429435	419894	410353	400813	394170	387526
610.93	466045	459751	453457	447163	440869	434575	428790	423005
616.48	483575	480527	477479	474432	471384	468337	463410	458483
622.04	498933	496257	493581	490905	488229	485553	481550	477546
627.59	514291	511986	509682	507378	505074	502770	499690	496609
633.15	529291	527257	525223	523189	521155	519121	516640	514158
638.71	543934	542068	540203	538338	536473	534607	532400	530192
644.26	558577	556880	555183	553487	551790	550094	548160	546227
649.82	572900	571305	569711	568116	566521	564926	563134	561341
655.37	587224	585731	584238	582745	581252	579759	578107	576456

Table A4 - Toluene Viscocity and Thermal Conductivity

Temp (°K)	Viscocity (kg/m-s)	Conductivity (W/m-°K)
488.71	0.0001060	0.10142
494.26	0.0001022	0.10020
499.82	0.0000984	0.09899
505.37	0.0000946	0.09778
510.93	0.0000908	0.09657
516.48	0.0000870	0.09536
522.04	0.0000832	0.09415
527.59	0.0000794	0.09294
533.15	0.0000756	0.09172
538.71	0.0000731	0.09034
544.26	0.0000705	0.08895
549.82	0.0000679	0.08757
555.37	0.0000654	0.08619
560.93	0.0000628	0.08480
566.48	0.0000605	0.08134
572.04	0.0000582	0.07788
577.59	0.0000561	0.07511
583.15	0.0000543	0.07303
588.71	0.0000525	0.07096
594.26	0.0000472	0.06680
599.82	0.0000419	0.06265
605.37	0.0000377	0.05884
610.93	0.0000345	0.05538
616.48	0.0000314	0.05192
622.04	0.0000294	0.04984
627.59	0.0000274	0.04777
633.15	0.0000256	0.04638
638.71	0.0000240	0.04569
644.26	0.0000223	0.04500
649.82	0.0000212	0.04517
655.37	0.0000202	0.04534

APPENDIX B - SIZING A HEAT EXCHANGER

To get an idea of the apporopriate operating range for the best performance from toluene, Rohsenow's Basic Methods [13] were modified to reflect the toluene properties with toluene thermal resistance dominating the heat transfer in the exchanger. The basic method develops correlations between the fluid properties, heat transfer, pressure loss with a tube and shell arrangement. Eight equations are manipulated so that a heat exchanger can be "sized" given the design requirements. Given the mass flow rates of the two fluids, the inlet temperature conditions, the temperature changes, and the allowed pressure loss, the complete details of the flow and dimension ratios are determined by selecting an hydraulic diameter. If the geometry is unsatisfactory, select a new diameter. This process is continued until an acceptable geometry is determined for further study.

The following series of equations are a simplification of the two fluid model and are based on the assumption that the cold side fluid controls the heat transfer.

GIVEN: m', T_{IN}, T_{OUT}, T_{HOT} (assumed constant), D,
allowable pressure loss, $h_{HOT} >> h_{COLD}$

CALCULATE:

$$\Delta T_{LM} = \frac{T_{OUT} - T_{IN}}{\ln\left(\frac{T_H - T_{OUT}}{T_H - T_{IN}}\right)} \qquad \text{and} \qquad q = m' \cdot C_{COLD} \cdot (T_{OUT} - T_{IN})$$

$$\dot{m}' = (\pi/4)\cdot D^2\cdot n\cdot G \qquad n\cdot G = \frac{\dot{m}'}{(\pi/4)\cdot D^2} = K1$$

$$q = \eta\cdot D\cdot L\cdot n\cdot h_c\cdot \Delta T_{LM} \qquad h\cdot n\cdot L = \frac{q}{\pi D\cdot \Delta T_{LM}} = K2$$

$$h\cdot D/k = 0.023\ Re^{0.8}\ Pr^{0.4} \qquad \frac{h}{G^{0.8}} = \frac{0.023\cdot k\cdot Pr^{0.4}}{D^{0.2}\cdot \mu^{0.8}} = K3$$

$$\Delta P = 4\cdot\left(\frac{0.046}{Re^{0.2}}\cdot\frac{L}{D}\cdot\frac{G^2}{2\cdot g_c\cdot\rho}\right) \qquad L\cdot G^{1.8} = \frac{\Delta P\cdot g_c\cdot\rho\cdot D^{1.2}}{0.092\cdot\mu^{0.2}} = K4$$

$$h\cdot n\cdot L = K2 = (K3\cdot G^{0.8})(K1/G)(K4/G^{1.8})$$

or

$$G = (K1\cdot K3\cdot K4/K2)^{1/2} = K7$$

$$n = K1/K7 \qquad L = K4/K7^{1.8}$$

The above sizing was performed for various values of hydraulic diameter. The toluene flow was divided into two sections and evaulated with the appropriate heat transfer coefficient for K3. Average fluid properties were assumed in each section. The result of this sizing indicated that pressure loss would be a smaller problem than inticipated in the reference cycle.

APPENDIX C - TOLUENE SIZING

As mentioned in Chapter 3, the toluene sizing model assumed a basic geometry (a square channel) as depicted in figure 11. This geometry was chosen because assembly difficulties were anticipated with very small finned tubes. Detailed here is the method used to size, with the formulas used and the values assigned.

The program is meant to determine optimum toluene flow parameters without assigning a specific geometry. To do this, input parameters were hydraulic diameter, Dh, and mass velocity, G. Output parameters were length, pressure, average heat transfer coefficient, and average fin effectiveness.

INPUT: Range of Dh and G to be swept and increment for integration, dL

ASSIGN:
- s' = 0.24812
- k_w = 127
- T_w = 650
- T_b = 488.71
- P = 4620
- fs = Dh
- fl = Dh/2 (Square passage)
- ft = Dh/5 (varied thickness later)

CALCULATE: Fluid Properties (Interpolation, see App A)
- $Re = G \cdot Dh/\mu$
- $f = 0.046/Re^{0.2}$
- $dP = 2 \cdot f \cdot dL/Dh \cdot G^2/\rho$
- $P = P - dP/1000$
- h_{TOL} = Swenson - McAdams if $T_b > 611$
- fe (as function if Dh and h_{TOL})
- $Q = h_{TOL} \cdot (T_w - T_b) \cdot dL \cdot (2\ fl\ fe + fs)$
- $T_b = T_b + Q/(G \cdot Cp \cdot fs \cdot fl)$

This process was repeated until T_b reached or surpassed 644°K.

APPENDIX D - TWO-PHASE MODEL FOR MERCURY

The following properties and equations were used to determine the significant flow properties of mercury [40,41,42]. As mentioned in chapter 4, the values represent fluid averaged properties based on quality. The homogeneous model assumes equal liquid and vapor velocities and calculates properties by adjusting the liquid only values by a correction factor, usually based on specific volumes and quality [24].

PROPERTIES: Evaluated at 654°K and 156 kPa

	liquid	vapor
Density (kg/m³)	12,678.7	5.7181
Viscocity (kg/m-s)	0.0008592	0.0000643
Thermal Conductivity (W/m-°K)	12.45	10.86
Specific Volume (m³/kg)	0.00007887	0.17488
Prandtl Number	0.0085	0.00059
Surface Tension	3871 N/m	
h_{FG}	294.75 kJ/kg	

TWO-PHASE FLOW VALUES

Density/volume $$v_m = \frac{1}{\rho_m} = [\, x \cdot v_v + (1-x) \cdot v_L \,]$$

Viscocity $$\frac{1}{\mu_M} = \frac{x}{\mu_v} + \frac{(1-x)}{\mu_L}$$

Friction Loss $$-\left(\frac{dp}{dz}\right)_{FR} = \left(\frac{dp}{dz}\right)_{FO} \cdot \left[1 + x \cdot \left(\frac{v_{Lv}}{v_L}\right)\right] \cdot \left[1 + x\left(\frac{\mu_{Lv}}{\mu_v}\right)\right]^{-1/3}$$

Momentum $$-\left(\frac{dp}{dz}\right)_{MOM} = G^2 \cdot v_{Lv} \cdot \left(\frac{dx}{dz}\right)$$

APPENDIX E - DETAILED HEAT BALANCE MODEL

This appendix lists the significant program steps which were used to perform a detailed heat balance between mercury and toluene. It is included because the quality distribution which was generated here was superimposed on the final design configuration. Besides the calculations for the final design performance, which were also a detailed heat balance, this program generated the most important data for the design of the unit.

Summarized below are the important program steps, leaving out file and printer commands and the interpolation subroutine.

```
Read data for interpolation
Dimension variables
Input:  m'TOL, m'HG, PTOT (start), fs, fl, ft, nt (# passages).
        spHG (HG outlet spacing), A4 (wall thickness)
Assign: property values
Calculate:  A1 = 2·fl/(2·fl+fs)          AF/AT
            A2 = (2·fl+fs)/(fs+ft)       AC/AH
            A6 = (fs+ft)·nt+(fs/2)       Width of toluene section
            A3 = A6·2                    Width of mercury flow
            A7 = spHG·A3                 Hg flow area (at exit)
            GHG = m'HG/A7                Hg mass velocity
            Dm = 2·spHG·A6/(A6+spHG)     Hg hydraulic diameter
            Rf = GHG·Dm/μL               Hg Liquid only Re
            N1 = 6.7+.0041·[(Rf·PrL)·793]·e(41.8 Pr)
                                         Liquid only Nusselt (Cohen)
Input:  Tw (guess), dL (integration step), TTOL, PTOL,
        X=0.852 (start values)

      DO WHILE TTOL < 644
GOSUB                                    -Inter S/R
Calculate:  vMHG                         -Mean Specific Volume
            hHG = h(z)·[(2-x)/(2+x)]     -Two-phase h adjusted by factor
            = N1·kL/Dm·[(vM/vL)1/2]·      to account for geometry
                       [(2-x)/(2+x)]     Geometry factor is removed
                                         when passage dimensions are
                                         applied in final configuration.
            Re = G·Dh/μ                  -Toluene Re
            f = 0.046/Re0.2              -Toluene f
            dP = 2·f·(dL/Dh)·G2·vTOL
            P = P-(dP/1000)              -New PTOL in kPa
            hTOL =                       -McAdams or Swenson
```

```
        BL = fl·[(h_TOL/k_MOLY·2/ft)^1/2]
        fe = [tanh(BL)]/BL
        Ec = 1-A1·(1-fe)              -Cold side effectiveness
        UA = 1/h_HG+A4/k_MOLY+1/(A2·h_TOL·Ec)
                                      -calc 1/U_H
        Q = (654-T_TOL)·dL·A3/UA      -Heat transferred in dL
        T_TOL = T_TOL+Q/(m'_TOL·Cp)   -Temp chg in dL
        Tw = Q/[h_TOL·nt·Ec·2·(2·fl+fs)·dL]
                                      -T_WALL for next section base on
                                       average flux out of toluene to
                                       total heating area
        L_TOT = L_TOT + dL
        X = X - Q/(h_FG·m'_HG)
LOOP
```

Other steps which were included in the above program kept track of total heat transferred by summing Q, change in bulk enthalpy, I_B, and total quality change. Average values of h_{TOL} and Ec were also calculated in an attempt at finding an approximate analytic solution. The following table summarizes some of the significant values.

Table E1 - Values Along Heating Length for Heat Balance (Parallel Flow)

Length (cm)	Temp (°K)	Press (kPa)	h_{TOL} (W/m²-°K)	Q (W)	h_{HG} (KW/m²-°K)	Quality (%)
Inlet	488.7	4413	-	-	-	0.852
10	529.6	4407	8227	2245	430.6	0.711
20	559.5	4401	8934	1804	451.5	0.584
30	580.3	4394	9591	1472	459.0	0.480
40	592.6	4386	10070	1254	455.3	0.382
50	598.3	4375	10150	1135	440.0	0.302
60	603.0	4361	16900	1422	421.3	0.245
70	610.2	4344	13470	1067	387.5	0.180
80	618.6	4324	11170	764	336.3	0.119
90	626.9	4300	10480	556	288.1	0.080
100	633.6	4275	10350	406	234.0	0.049
110	638.7	4249	10390	295	177.3	0.026
120	642.4	4223	10470	207	112.3	0.009
126	644.0	4207	10510	150	60.0	0.000

The values above are not those of the final configuration, but are representative of the final calculations.

APPENDIX F - RECOMMENDED EXPERIMENT FOR HEAT TRANSFER COEFFICIENTS

The main uncertainties in this design are the heat transfer coefficients of toluene and condensing mercury. The data from SNAP-8 is well documented, but it deals primarily with flows condensing in tubes. As far as this author could tell, supercritical heat transfer tests with toluene have not been conducted. The use of the Swenson correlation is therfore tenuous at best.

Recommend testing to verify the heat transfer correlations for the two fluids with plate-fin geometries. Additionally, recommend that mercury be tested with a variable geometry applied to the flow passage. In this manner, differences in heat transfer may be more closely linked to pressure changes and flow acceleration. It may be possible to test the two fluids together, but it is probably not necessary. Possible flow configurations could be; mercury boiling toluene, condensing mercury boiling toluene, mercury heating supercritical toluene, and condensing mercury heating supercritical toluene.

The primary objective will be to validate the plot of toluene heat transfer prediction in the supercritical pressure region near the specific heat spike when wall and fluid temperatures are on opposite sides of the specific heat spike.

REFERENCES

1. Fox, Allen G. and Jean F. Louis, "Specific Mass and Cogeneration," unpublished, undated article, M.I.T., Cambridge, MA.

2. Fox, Allen G., "A Conceptual Study of a Solar Power System Based on a Combined Mercury-Toluene Rankine Cycle," Masters Thesis, Department of Mechanical Engineering, M.I.T., Cambridge, MA, January, 1987.

3. Chaudoir, D.W., et al., "A Solar Dynamic ORC Power System for Space Station Application," Sunstrand Corp., Rockford, IL, 1985.

4. Bland, Timothy J., et al., "A Two-Phase Thermal Management System for Large Spacecraft," SAE-851351, July, 1985.

5. Gieck, Kurt, Engineering Formulas, 5th ed., McGraw-Hill, New York, 1986

6. Akkerman, J.W., "Space Station Systems Engineering Approach", Proceedings of the Workshop on Dynamic Power Systems for Space Station, 31 January - 2 February 1984.

7. Swenson, H.S., et al., "Heat Transfer to Supercritical Water in Smooth Bore Tubes," Journal of Heat Transfer, trans. ASME-87, 1965.

8. Personal Communication with Professor Jean F. Louis, Department of Aeronautics and Astronautics, M.I.T., Cambridge, MA, Nov, 1986.

9. Kays, William M. and H.C. Perkins, "Forced Convection, Internal Flows in Ducts," in Handbook of Heat Transfer, McGraw-Hill, NY, 1973.

10. Personal Communication with Peter Griffith, Professor, Department of Mechanical Engineering, M.I.T., Cambridge, MA, 23 February 1987.

11. Shiralkar, Bharat S. and Peter Griffith, "The Deterioration in Heat Transfer to Fluids at Super-Critical Pressure and High Heat Fluxes," Heat Transfer Laboratory Report no. 70332-51, March 1, 1968.

12. Shiralkar, Bharat S. and Peter Griffith, "The Deterioration in Heat Transfer to Fluids at Super-Critical Pressure and High Heat Fluxes," Heat Transfer Laboratory Report no. 70332-55, June 30, 1968.

13. Rohsenow, Warren M., "Heat Exchangers-Basic Methods", Department of Mechanical Engineering, M.I.T., Cambridge, MA, undated.

14. Rohsenow, Warren M., "Heat Transfer and Pressure Drop", Addendum to Basic Methods, undated.

15. Rohsenow, Warren M. and L.S. Cohen, M.I.T. Heat Transfer Laboratory Report, June, 1960.

16. Metals Handbook, vol. 2, Nonferrous Alloys and Pure Metals, 9th ed., American Society for Metals, Metals Park, Ohio, 1979.

17. Metals Handbook, vol. 3, Stainless Steels, Tool Materials and Special Purpose Metals, 9th ed., American Society for Metals, Metals Park, Ohio, 1980.

18. Lottig, Roy A., et al., "Experimental Heat-Transfer Investigation of Nonwetting, Condensing Mercury Flow in Horizontal, Sodium-Potassium-Cooled Tubes," NASA TN D-3998, May, 1967.

19. "SNAP-8 Electrical Generating System Development Program," Aerojet-General Corporation, NASA CR-1907, November, 1971.

20. Koestel, Alfred, et al., "Study of Wetting and Nonwetting Mercury Condensing Pressure Drops," NASA TN D-2514, November 1964.

21. Albers, James A., et al., "Experimental Pressure-Drop Investigation of Nonwetting Condensing Flow of Mercury Vapor in Constant-Diameter Tube in 1-G and Zero Gravity Environments," NASA TN D-2838, June, 1965.

22. Albers, James A., and Henry B. Block, "Experimental Pressure Drop Investigation of Wetting and Non-Wetting Mercury Condensing in Uniformly Tapered Tubes," NASA Tn D-3253, February, 1966.

23. Namkoong, D., et al., "Photographic Study of Condensing Mercury Flow in 0-G and 1-G Environments," NASA TN D-4023, June, 1967.

24. Collier, John G., Convective Boiling and Condensation, 2nd ed., McGraw-Hill, Berkshire, UK, 1981.

25. Rohsenow, Warren M. and Harry Choi, Heat, Mass, and Momentum Transfer, Prentice-Hall, Englewood Cliffs, NJ, 1961.

26. Griffith, Peter, "Two-Phase Flow," in Handbook of Heat Transfer, McGraw-Hill, NY, 1973.

27. Koestel, Alfred, et al., "Study of Wetting and Nonwetting Mercury Condensing Pressure Drops," NASA TN D-2514, November 1964.

28. Kays, W.M., and A.L. London, Compact Heat Exchangers, 3rd ed., McGraw-Hill, New York, 1984.

29. Rohsenow, Warren M., Material from handouts from M.I.T. course 2.601J, Thermal Power Systems, Spring 1987.

30. Personal communications with Warren M. Rohsenow, Professor of Mechanical Engineering, M.I.T., Cambridge, MA, Feb-May, 1987.

31. Fontana, Mars G., Corrosion Engineering, 3rd ed., McGraw-Hill, NY, 1986.

32. Stevens, Karl K., Statics and Strengths of Materials, Prentice-Hall, Englewood Cliffs, NJ, 1979.

33. "Micrometeoroid Environment," unknown source, handout material for M.I.T. course 16.042, Fall, 1986.

34. Collins, J.A., Failure of Materials in Mechanical Design, John Wiley and Sons, NY, 1981.

35. "Meteoroid Environment Model - 1969," NASA SP-8013, March 1969.

36. Personal communication with Thomas W. Eagar, Associate Professor of Materials Engineering, M.I.T., Cambridge, MA, 24 April 1987.

37. Lindberg, Roy A. and Norman R. Braton, Welding and Other Joining Processes, Allyn and Bacon, Boston, 1976.

38. Computer generated tables of toluene data provided to Professor Jean F. Louis by Sunstrand Technologies Group, Rockford, IL.

39. Touloukian, Y.S., et al., Thermophysical Properties of Matter, vol.3, Thermal Conductivity: Nonmetallic Liquids and Gases, Plenum Publishing, NY, 1970.

40. Touloukian, Y.S., et al., Thermophysical Properties of Matter, vol.11, Viscocity, Plenum Publishing, NY, 1970.

41. Reynolds, W.C., Thermodynamic Properties in SI, Stanford University Press, 1979.

42. Touloukian, Y.S., et al., Thermophysical Properties of Matter, vol.1, Thermal Conductivity: Metallic Elements and Alloys, Plenum Publishing, NY, 1970.